Close association between altered urine–urothelium barrier and tertiary lymphoid structure formation in the renal pelvis during nephritis

Osamu Ichii[1,2*], Marina Hosotani[3], Md. Abdul Masum[1,4], Taro Horino[5], Teppei Nakamura[1,6], Takashi Namba[1], Yuki Otani[1], Yaser Hosny Ali Elewa[1,7], and Yasuhiro Kon[1]

[1]Laboratory of Anatomy, Department of Basic Veterinary Sciences, Faculty of Veterinary Medicine, Hokkaido University, Sapporo, Japan 060-0818

[2]Laboratory of Agrobiomedical Science, Faculty of Agriculture, Hokkaido University, Sapporo, Japan 060-8589

[3]Laboratory of Anatomy, School of Veterinary Medicine, Rakuno Gakuen University, Ebetsu, Japan 069-8501

[4]Department of Anatomy, Histology and Physiology, Faculty of Animal Science and Veterinary Medicine, Sher-e-Bangla Agricultural University, Dhaka, Bangladesh 1207

[5]Department of Endocrinology, Metabolism and Nephrology, Kochi Medical School, Kochi University, Nankoku, Japan 780-8072

[6]Section of Biological Safety Research, Chitose Laboratory, Japan Food Research Laboratories, Chitose, Japan 066-0052

[7]Department of Histology, Faculty of Veterinary Medicine, Zagazig University, Zagazig, Egypt 44519

Running title: Lymphoid structures in renal pelvis

*Correspondence to Osamu Ichii (DVM, PhD); ORCID:0000-0002-6643-1554

Laboratory of Anatomy, Department of Basic Veterinary Sciences, Faculty of Veterinary Medicine, Hokkaido University, Kita 18, Nishi 9, Kita-ku, Sapporo 060-0818, Japan

Tel/Fax: +81-11-706-5189; Email: ichi-o@vetmed.hokudai.ac.jp

Keywords: tertiary lymphoid structure, renal pelvis, urine, urothelium, nephritis, chemokine

Abstract

Background: Kidneys with chronic inflammation develop tertiary lymphoid structures (TLSs). Infectious pyelonephritis is characterized by renal pelvis (RP) inflammation. However, the pathological features of TLS including its formation and association with non-infectious nephritis are unclear.

Methods: RPs from healthy humans and mice, and those from humans and mice with non-infectious chronic nephritis were pathologically analyzed for TLS development, and the mechanism of TLS formation was investigated using urothelium or lymphoid structure cultures.

Results: Regardless of infection, TLSs in the RP, termed urinary tract-associated lymphoid structures (UTALSs), formed in humans and mice with chronic nephritis. Moreover, urine played a unique role in UTALS formation. Specifically, urinary IFN-γ was identified as a candidate factor affecting urothelial barrier integrity by altering occludin expression. Urine leakage from the lumen of the RP into the parenchyma was demonstrated in a nephritis mouse model. Moreover, urine immunologically stimulated UTALS-forming cells via cytokine (IFN-γ, TNF-α) and chemokine (CXCL9, CXCL13) production. CXCL9 and CXCL13 were expressed in UTALS stromal cells, and urine stimulation specifically induced CXCL13 in cultured fibroblasts. Characteristically, type XVII collagen (BP180), a candidate autoantigen of bullous pemphigoid, was ectopically localized in the urothelium covering UTALSs and associated with UTALS development by stimulating CXCL9 or IL-22 induction via the TNF-α/FOS/JUN pathway. Notably, UTALS development indices were positively correlated with chronic nephritis development.

Conclusion: TLS formation in the RP is possible and altered urine–urothelium barrier-based UTALS formation may represent a novel mechanism underlying the pathogenesis of chronic nephritis, regardless of urinary tract infection.

Introduction

Systemic lymphoid tissues (LTs) of mammals are classified into primary LT, secondary LT, and tertiary lymphoid structures (TLSs) based on their localization, function, or manner of development.[1] Bone marrow and thymus constitute primary LTs, whereas spleen, lymph nodes, and mucosa-associated LTs (MALTs) constitute secondary LTs. TLSs are found in systemic organs and their formation is related to chronic inflammation associated with cancer, and autoimmune disease (AID) or allergic disease.[2,3] Recent studies have emphasized the importance of TLSs found in the kidney parenchyma of elderly individuals and nephritis patients.[4,5] Moreover, TLS development may lead to chronic kidney disease,[5] whose global prevalence has increased and evolved into a serious public health challenge often associated with end-stage renal disease.[6] In particular, stromal immunofibroblasts,[7] which produce chemokines (CCL20 and CXCL13), may play a principal role in renal TLS formation by attracting immune cells *in situ*.[5,8,9]

Kidneys are linked to the outer environment via the urinary tract (UT). The renal pelvis (RP), a border structure that exists between the kidney and the UT, receives urine. As a portion of the RP penetrates deep into the kidney, the RP is intricately connected to the renal parenchyma via connective tissues. Primarily, UT infections that disrupt the barrier function of the urothelium lining the RP cause inflammatory lesions in the RP and renal parenchyma, leading to pyelonephritis.[10] The mortality rate associated with severe pyelonephritis exceeds 20%.[11] Renal parenchymal inflammation caused by non-infectious inflammatory conditions such as AID may cause glomerular and tubulointerstitial inflammation.[12] Although MALTs do not form in the RP under non-infectious conditions, the possibility of their formation nevertheless exists as the urothelium and RP are intricately connected, similar to the intricate connection between the epithelium and parenchyma in organs with MALT. Nevertheless, MALT lymphoma can develop in the human RP.[13] Age-related TLS formation may be observed in the urinary bladder even under non-infectious conditions.[14] These clinical findings suggest that lymphoid structure (LS) formation in the UT, including the RP, is possible.

Here we aimed to examine LS formation in the RP under normal and disease conditions in both humans and mice, and investigate other factors that may be involved in LS development to demonstrate the pathological association between non-infectious chronic nephritis and LS formation in the RP.

Materials and methods

Human sample analysis

We obtained 10% neutral buffered formalin (NBF)-fixed, paraffin-embedded, normal kidney tissues (two Caucasian females, 33 and 34 years), and kidney samples of infectious pyelonephritis (Caucasian male, 39 years) and non-infectious chronic nephritis (two Caucasian males, 69 and 52 years and an Asian male, 53 years) from KAC Inc. (Kyoto, Japan). Urine was collected from healthy human volunteers from Hokkaido University (*n* = 10, average age = 27 years) or patients with AID-related nephritis at Kochi University (*n* = 12, average 47 years). Written informed consent from the donors, next of kin, or persons exercising parental authority for minors was obtained. The study of human samples was approved by the Ethics Committee of Kochi University (approval no. 24-134). Analyses of human samples were approved by the Ethics committee of the Faculty of Veterinary Medicine and Research Center for Zoonosis Control, Hokkaido University (approval no. 29-5). The collection of samples from human subjects was performed in accordance with the Declaration of Helsinki and Declaration of Istanbul.
Paper urinalysis was performed using Multistix PRO11 (Siemens Healthcare, Tokyo, Japan). Paper urinalysis did not indicate remarkable differences in pH (6.5 vs 7.0) or gravity (1.02 vs 1.02) of the pooled urine between healthy controls and patients with nephritis. The urine samples were analyzed using a Human ProQuantum Immunoassay Kit for IFN-γ and TNF-α (#A35576, #A35601; Thermo Fisher Scientific, Waltham, MA, USA).

Animals and sample preparation

C57BL/6N of both sexes, female MRL/MpJJmsSlc (MRL/MpJ) and MRL/MpJJmsSlc-*lpr/lpr* (MRL/lpr), and male BXSB/MpJ and BXSB/MpJ-*Yaa* were purchased from Japan SLC Inc. (Shizuoka, Japan) and used at the age of 2, 3, 9, and 12 months (C57BL/6N), 3 months (MRL/lpr), and 6 months (all strains). Female B6.MRLc1 were maintained in our laboratory[15] and used at the age of 9 months. Animal experimentation procedures were approved by the Institutional Animal Care and Use Committee of the Graduate School of Veterinary Medicine,

Hokkaido University (approval no. 16-0124). Investigators adhered to the Guidelines for the Care and Use of Laboratory Animals of Hokkaido University, Faculty of Veterinary Medicine. All animal experimental protocols were approved by the Association for Assessment and Accreditation of Laboratory Animal Care International. All mice used in this study were euthanized by cutting the femoral artery under deep anesthesia (0.3 mg/kg medetomidine, 4.0 mg/kg midazolam, and 5.0 mg/kg butorphanol). For 2-month-old C57BL/6N, unilateral ureter obstruction (UUO) for 1 day or its equivalent sham operation was performed under deep anesthesia. The number of animals used for each experiment is described in each figure legend. After euthanasia, spleen to body weight ratio (SPW/BW) was calculated, and serum double-stranded DNA auto-antibody levels were measured using an ELISA kit (#82639; Immuno-Biological Laboratories, Gunma, Japan). Kidneys were collected, cut into four transverse quarter sections, and fixed in either 4% paraformaldehyde (PFA)/0.1 M phosphate buffer (PB) for histological analysis or in 2.5% glutaraldehyde (GTA) for scanning electron microscopy (SEM) analysis. A part of the kidney was stored in RNAlater (Thermo Fisher Scientific) for gene expression analysis.

Histopathology

Histological sections of human kidney were stained using Masson's trichrome (MT) or periodic acid Schiff (PAS), while mouse kidneys were stained using hematoxylin and eosin (H&E), MT, PAS, or silver impregnation. Immunohistochemistry (IHC) and immunofluorescence (IF) were performed as previously described.[16] Information regarding antigen retrieval and antibodies used is summarized in **Supplemental Table 1**. Stained sections were examined using a BZ-X710 microscope (Keyence, Osaka, Japan) and converted to virtual slides using NanoZoomer 2.0-RS (Hamamatsu Photonics, Shizuoka, Japan). *In situ* hybridization (ISH) was performed using RNAscope (R) 2.5 HD Reagent Kit-BROWN (#322300; Advanced Cell Diagnostics, Newark, CA, USA) and HybEZ™ II Hybridization System with EZ-Batch Slide System (Advanced Cell Diagnostics) as previously described.[17] The probes used in this study are listed in **Supplemental Table 2**.

For localization analysis of LSs formed in the RP, semi-serial sections were obtained from the cranial to caudal poles of a 6-month-old male C57BL/6N kidney at 70 μm intervals and stained using H&E. These sections were converted into virtual slides using NanoZoomer 2.0-RS and observed using the NDP.view2 program (Hamamatsu Photonics). LSs in the abdominal, central, and dorsal RPs in each section were counted (**Supplemental Figures 1, 2A**).

Histoplanimetry

The glomerular area and the number of $CD3^+$ or $B220^+$ cells in the glomerular sections obtained from a 6-month-old mouse kidney were quantified via IHC using the BZ-H3C analysis application. Digital images were obtained using the BZ-X710 microscope. For glomerular lesions (GLs), the number of positive cells was divided by the glomerular area to obtain the density of positive cells in the glomerulus. For TLS formation, digital images of kidney sections stained for CD3 or B220 in IHC were obtained using NDP.view2 at 0.36-fold magnification. The digital images were converted to binary images, and the area of clusters positive for CD3 or B220 in the areas of kidney sections without LSs formed in the RP was measured using Image J (National Institutes of Health, Bethesda, MD, USA). For tubulointerstitial lesions (TILs), images of tubulointerstitial regions that did not contain glomeruli were obtained with NDP.view2, converted to binary images, and then integrated density (IntDen) of $CD3^+$ or $B220^+$ reactions in the unit area was quantified via Image J. The number of $CD3^+$ or $B220^+$ cells in the examined RP area was quantified in 9-month-old C57BL/6N and B6.MRLc1.

For collagen type XVII alpha 1 chain (COL17A1) IHC, images of LSs formed in the RPs were randomly obtained by NDP.view2, converted to binary images, and then IntDen of $COL17A1^+$ reactions in urothelium was quantified using Image J. These values were divided by the IntDen of nuclei stained by hematoxylin in the examined area of LSs formed in the RP or the examined LS area.

SEM

GTA-fixed kidneys were post-fixed with 1% OsO_4 at 4 °C for 1 h, washed with 0.1 M PB, and treated with 1% tannic acid at 4 °C for 1.5 h. After washing with 0.1 M PB, the specimens were dehydrated via an ascending alcohol gradient, transferred into 3-methylbutyl acetate, and finally dried (HCP-2 critical point dryer; Hitachi, Tokyo, Japan). The dried samples were fixed on aluminum stubs with double-faced adhesive tabs. Surface treatment with a platinum layer was performed with ion sputtering (E-1030; Hitachi), and the samples were observed via SEM (SU8000; Hitachi).

Mimic LS (mLS) culture and analysis

The spleen of a 6-month-old mouse was collected and minced in a culture dish. Next, 10 mL of 1X phosphate buffered saline (-) (PBS, #164-25511; FUJIFILM Wako, Osaka, Japan) was added, after which the sample was filtered using 100 μm cell strainers (#352360; Corning Inc., Corning, NY, USA) and centrifuged at 1,000 rpm for 5 min. After supernatant aspiration, cells were resuspended, incubated with 10 mL of 0.017 M tris buffer containing 0.75% ammonium chloride (pH 7.65) for 5 min, and washed with 10 mL PBS. This solution was filtered using 40 μm cell strainers (#352340; Corning Inc.) and centrifuged at 1,000 rpm for 5 min. After washing twice with PBS, the collected cells were resuspended in RPMI1640 with L-glutamine (#189-02025; FUJIFILM Wako) without antibiotics and harvested in 24-well culture plates (#92424; Techno Plastic Products, Trasadingen, Switzerland).

The cells were defined as mLSs containing immune and stromal cells. Furthermore, some spleen cells were similarly collected without ammonium chloride treatment, and then T, B, and $CD11b^+$ cells were separately isolated using magnetic-activated cell sorting-based commercial kits (EasySep, #ST-19851RF, #ST-19854RF, #ST-18970RF; VERITAS, Santa Clara, CA, USA). mLSs or separated cells were stimulated using recombinant human COL17A1 (rhCOL17A1; #MBS1265558; MyBioSource, San Diego, CA, USA) or bovine serum albumin (BSA; #013-27054; FUJIFILM Wako). Endotoxin levels in rhCOL17A1 were <1.0 endotoxin unit per 1.0 μg protein as determined using a limulus amebocyte lysate test (MyBioSource). Urine was collected

from five MRL/MpJ or MRL/lpr at 6 months of age via compressive urination, after which samples from each strain were pooled and centrifuged at 1,500 rpm for 5 min. Paper urinalysis was performed using Multistix PRO11. The urine supernatant was filtered using a 0.22 μm syringe filter (#SLPES2522S; Hawach Scientific, Shaanxi, China) and used for mLS stimulation. mLS or isolated cell experiments were performed using 2.5×10^7 cells/mL and 500 μL medium/well or 2.5×10^7 cells/mL and 500 μL medium/well, respectively.

After rhCOL17A1 or BSA treatment, mLS cell viability was analyzed via the CellTiter 96®AQueous One Solution Assay (#G3582; Promega, Madison, WI, USA). After stimulation with rhCOL17A1 or urine, the culture supernatant was collected, centrifuged at 2,000 rpm for 5 min, and analyzed using mouse ELISA kits for IL-6 (#27768; Immuno-Biological Laboratories), IFN-γ or TNF-α (#630-44701 or #634-44721; FUJIFILM Wako), and CXCL9 or CXCL13 (#MCX900 or #MCX130; R&D Systems, Minneapolis, MN, USA). Cells were then collected for quantitative PCR (qPCR). For IF, the stimulated mLSs were embedded in iPGell (#PG20-1; GenoStaff, Tokyo, Japan), fixed with 4% PFA/0.1 M PB, and paraffin embedded. Histological sections were stained according to appropriate antigen retrieval conditions and antibody dilutions (**Supplemental Table 1**).

Cell culture and analysis

NIH3T3 cells (RIKEN Bioresource Center, Tsukuba, Japan) were maintained in DMEM (#041-29775; FUJIFILM Wako) supplemented with 10% fetal bovine serum (FBS; #10099141; Thermo Fisher Scientific) and 1X penicillin/streptomycin (Thermo Fisher Scientific) until reaching 70% confluency. NIH3T3 cells were resuspended in DMEM without FBS and antibiotics and cultured in 24-well culture plates until 90% confluency. After 24 h, the cells were stimulated using rhCOL17A1, BSA, or 25% MRL/MpJ or MRL/lpr urine diluted with DMEM for 3 h as described for mLS culture. The culture supernatant was collected, centrifuged at 2,000 rpm for 5 min, and analyzed using mouse ELISA kits for CXCL13 (#MCX130; R&D Systems). Cells were collected by scraping for qPCR. For IF, stimulated NIH3T3 cells were analyzed as described for mLSs.

Normal human urothelial cells (HUCs; #KP-4109; Kurabo, Osaka, Japan) were maintained in a UroLife Comp kit (#LUC-LL0071; Kurabo) until 100% confluency. HUCs were cultured in 6-well culture plates (#92406; Techno Plastic Products) or on cover glasses placed within microplate wells for IF. The medium was changed to basal medium (UroLife BM; #LUC-LL0054; Kurabo) without growth factors. After 24 h, HUCs were stimulated using 25% human urine diluted with basal medium for 3 h or 1.0 ng human recombinant IFN-γ or TNF-α (#285-IF or #210-TA; R&D Systems) for 24 h. Cells were collected by scraping for qPCR. HUCs were fixed using methanol/acetone at 4 °C for 30 min, and then IF was performed as previously described.[18] Information regarding antibodies used is summarized in **Supplemental Table 1**.

RNA analysis

Using a stereo microscope, the RP was isolated by microdissection from the stored kidney section in RNAlater (**Supplemental Figure 2B**). Then, total RNA was purified from the kidney section, separated RP, and cultured cells using the TRIzol reagent (#15596018; Thermo Fisher Scientific). Purified total RNA was used as a template to synthesize cDNA using ReverTra Ace® qPCR RT Master Mix with gDNA Remover (#FSQ-301; Toyobo, Osaka, Japan). Products amplified by PCR using GoTaq® Green Master Mix (#M7121; Promega, Madison, WI, USA) and gene-specific primers (**Supplemental Table 2**) were visualized with 2% agarose gel electrophoresis.

QPCR analysis was performed using the THUNDERBIRD® SYBR® qPCR Mix (#QPS-101; Toyobo), gene-specific primers (**Supplemental Table 2**), and a real-time thermal cycler (CFX Connect; BIO-RAD, Santa Rosa, CA, USA). Cycle conditions are listed in **Supplemental Table 2**. Data were normalized to the values of actin beta (*Actb*) or uroplakin 3 (*Upk3*) in mice, glyceraldehyde-3-phosphate dehydrogenase (*GAPDH*) in human cells, and to those of control expression using the delta-delta Ct method.

Microarray

Total RNA was purified from animal tissues stored in RNAlater or cultured mLS cells using the RNeasy Mini Kit (#74104; Qiagen, Hilden, Germany). For kidneys, RNA from MRL/MpJ (*n* = 7) and MRL/lpr (*n* = 10) mice was pooled into one sample for each group. The RNA of mLS cells was also prepared from the PBS- or rhCOL17A1-treated group (*n* = 3). RNA integrity was validated using an Agilent 2100 Bioanalyzer II (Agilent Technologies, Santa Clara, CA, USA); complementary RNA was synthesized using a Low Input Quick Amp Labeling Kit (Agilent Technologies), whereas gene expression was analyzed using an Agilent Technologies Microarray Scanner and SurePrint G3 Mouse 8x60K ver.2.0 (Agilent Technologies). Obtained raw data were normalized using 75Percentile Shift (GeneSpring; Agilent Technologies). Minimum information about a microarray experiment-compliant dataset was deposited in the NCBI Gene Expression Omnibus and is accessible under the GEO Series accession numbers GSE151929 and GSE151930. STRINGs (https://string-db.org/) was used for gene ontology (GO) analysis. RP samples highly expressed urothelium markers, indicating their successful isolation from mouse kidneys (**Supplemental Table 3**).

Urothelium integrity analysis

Evans blue (5 mg/mL; #E2129; Merck, Kenilworth, NJ, USA) was mixed with BSA (40 mg/mL), incubated for 30 min, and filtered using a 0.22 μm syringe filter to produce Evans blue-conjugated BSA (EBA) solution. The urethra of female mice was ligated under combination anesthesia (0.3 mg/kg medetomidine, 4.0 mg/kg midazolam, and 5.0 mg/kg butorphanol), and a 20 G feeding needle was inserted from the apex of the urinary bladder and fixed via ligation. After clamping one ureter with vascular clips (KN-353-AS-1-40 g; Natsume Seisakusho, Tokyo, Japan), 50 μL EBA was injected into the urinary bladder through an inserted feeding needle. EBA injection to the RP was confirmed via color change in the other ureter (**Supplemental Figure 3**). After 5 min of contact time, the mice were euthanized, and 4% PFA/0.1 M PB was perfused from the left ventricle to systemic circulation. Next, the kidneys were immediately collected, and embedded in OCT compound (#4583; Sakura Finetek Japan, Tokyo, Japan) using liquid nitrogen. Frozen

sections (4 μm) were prepared, fixed with 4% PFA/0.1 M PB for 5 min, washed with PBS and then distilled water, and finally air dried. The EBA fluorescence signal was observed using the BZ-X710 microscope and Cy5 filter. Obtained images were converted to binary images, and the relative area of EBA in RP to urothelium length along with the examined area was quantified using Image J.

Statistical analysis

For two-group comparisons, Student's *t*-test or Mann–Whitney *U*-test was used for microarray analysis and other experiments, respectively. For multiple comparisons, Dunnett's test was performed when statistical significance was observed with the Kruskal-Wallis test. Spearman's correlation tests were used to analyze the correlation between two parameters. *P* values <0.05 were considered statistically significant.

Results

LSs form in the human RP

Patients diagnosed with either infectious pyelonephritis or non-infectious chronic nephritis showed severe TILs and GLs (**Figure 1A**). MT staining showed well-developed collagen fibers beneath the RP urothelium in the normal kidney (**Figure 1B**). In both patients, these fibers were reticularly distributed in the RP, while numerous infiltrating $CD3^+$ T cells (**Figure 1C**), $CD20^+$ B cells, and $IBA1^+$ macrophages (**Supplemental Figure 4**) were found between fibers and in the urothelium. Type III collagen $(COL3A1)^+$ reticular fibers were localized in all examined RPs (**Figure 1D**). Furthermore, several $PNAd^+$ high endothelial venules (HEVs), entrances for immune cells, were observed in the RP of both patients (**Figure 1E**).

In the absence of infection, necropsy samples showing normal histology, moderate chronic nephritis, or severe chronic nephritis also revealed scarce, moderate, or abundant cell infiltration of RPs, respectively (**Figure 1F, G**). These structures were termed UT-associated LSs (UTALSs) and the mechanism underlying their formation was investigated in subsequent experiments.

UTALSs form in the RP of healthy and nephritis mice

Histological analysis using semi-serial sections of 6-month-old C57BL/6N kidneys demonstrated UTALS localization in the deep portion of RP (**Figure 2A, Supplemental Figures 1, 2A**). Gene expression analysis revealed that T and B cells, macrophages, and antigen-presenting cells (APCs) were abundantly localized in the RP (**Figure 2B**).

Small UTALSs were composed of condensed collagen fibers, several $CD3^+$ T cells, $B220^+$ B cells, $IBA1^+$ macrophages, $Ly\text{-}6G^+$ granulocytes, and $LYVE1^+$ lymphatic vessels (LVs) (**Supplemental Figure 5**). Large UTALSs comprised abundant immune cells—consisting of T cells, B cells, and macrophages similar to human UTALSs—occupying spaces between developed connective tissue fibers (**Figure 2C, D, Supplemental Figure 6A)**. Well-developed $COL3A1^+$ fibers and $PNAd^+$ HEVs were detected in the UTALSs (**Figure 2E, F**). Additionally, large UTALSs consisted of several LVs and $FOXP3^+$ regulatory T cells (**Supplemental Figure**

6B). Twelve-month-old C57BL/6N developed large UTALSs (**Supplemental Figure 6C**–**F**), suggesting the effect of age-related factors on their development.

The other glomerulonephritis model BXSB/MpJ-*Yaa* (**Supplemental Figure 7**) and B6.MRLc1, a mouse model of C57BL/6N-background spontaneous chronic glomerulonephritis,[15] showed increased lymphocyte numbers in the RP (**Figure 2G, H**).

UTALSs develop in the RP of a severe nephritis mice

Next, we examined MRL/lpr, a representative severe immune-mediated nephritis model. Compared with control MRL/MpJ, MRL/lpr exhibited significantly higher histopathological indices of GL, TIL, and TLS formation in the kidney (**Supplemental Figure 8A–C**). MRL/lpr developed nephritis with large UTALSs that consisted of B cells, T cells, macrophages, APCs, LVs, and HEVs (**Figure 3A–D**). Immune cell marker expression was significantly higher in the RP than in the MRL/MpJ kidney, and significantly higher in the kidney and RP of MRL/lpr compared with MRL/MpJ (**Figure 3E**). Furthermore, there was a significant correlation between GL, TIL, or TLS indices and *Il2ra*, *Cd3e*, or *Ptprc* expression in RPs (**Table 1**).

UTALS of MRL/lpr at 3 months was smaller than at 6 months but larger than in same-aged healthy mice (**Supplemental Figure 6, 9**). Moreover, 3-month-old MRL/lpr manifested AID,[16] suggesting the involvement of systemic immune factors in UTALS development.

Altered urothelium barrier (UB) of the RP in mice and humans showing nephritis

UTALSs are in proximity with the RP lumen through the urothelium. Although aging and AID are well-established factors that contribute to the development of TLS,[4,5] we hypothesized that UB integrity in the RP is altered under nephritic conditions, resulting in subsequent leakage of urine into the RP that may in turn contribute to UTALS development. To assess this phenomenon, we examined UBs in the RP. After 1 day of UUO in young C57BL/6N (2-month-old), the RP showed mild cellular aggregation in the RP parenchyma with decreased staining intensity of tight junction (TJ) molecules such as occludin (OCLN) and ZO-1, suggesting an association between UTALS

formation and altered UB; however, UTALS size was smaller compared with that in aged or AID mice (**Supplemental Figure 6, 9, 10**). To clearly characterize the association between UB integrity and UTALS formation, subsequent experiments were performed using MRL/MpJ and MRL/lpr.

The urothelium surface in MRL/MpJ was wrinkled at low magnification and the cell surface was irregular; however, the RP wall was thicker in MRL/lpr than in MRL/MpJ, several epithelial cells were absent, and alterations to the spherical or domed shape were observed in the RP epithelium of MRL/lpr (SEM; **Figure 4A–C**).

Based on microarray data (**Supplemental Data 1**), the expression of urothelium markers and TJ molecules decreased in the RP of MRL/lpr compared with that of MRL/MpJ (**Supplemental Table 4**). QPCR of selected genes identified using microarray confirmed that occludin (*Ocln*) levels significantly decreased in the RP of MRL/lpr compared with MRL/MpJ (**Figure 4D**).

In MRL/MpJ, ZO-1 and OCLN localized to the urothelium in the RP, as $OCLN^+$ staining showed a linear pattern at the apical side (**Figure 4E**). However, in MRL/lpr, $OCLN^+$ staining was faint and localized in the basal portion of the urothelium, while some parts of the urothelium invaginated toward the RP. Furthermore, some $ZO\text{-}1^+$ staining patterns in the urothelium were discontinuous instead of linear. In human patients (**Figure 4F**), TJ localization patterns were altered, showing discontinuous $ZO\text{-}1^+$ staining and $OCLN^+$ cells that were localized to the basal side and other areas of the urothelium, compared with normal human kidneys. Retrograde EBA administered from the urinary bladder to RP (**Supplemental Figure 3**) was retained and observed in the urothelium of MRL/MpJ RP; however, EBA significantly leaked into some parts of the developing UTALS in the MRL/lpr RP (**Figure 4G, H**).

Next, we assessed TNF-α and IFN-γ as candidates for UB defects based on previous organ studies.[19–21] Urine TNF-α and IFN-γ were significantly upregulated in patients with non-infectious nephritis than in healthy controls, while cultured HUCs expressed one and two types of TNF-α and IFN-γ receptor genes, respectively (**Figure 5A, B**). *OCLN* expression in HUCs significantly decreased after stimulation with IFN-γ or urine from nephritis patients (**Figure 5C, D**). While non-

simulated HUCs formed several clusters with linear localization of TJ proteins, these clusters significantly decreased in size and number after IFN-γ stimulation (**Figure 5E, F**).

Candidate molecules associated with UTALS development

Next, we examined the response of cells composing UTALSs after urine stimulation. First, we performed microarray analysis using the RP and kidneys of MRL/MpJ or MRL/lpr (**Supplemental Data 1**). Using MRL/MpJ data, we detected several immune-associated GO terms, and STRING analysis of upregulated gene sets in the RP showed a large cluster of chemokines and associated receptor genes (**Supplemental Figure 11A–C**), which are crucial in attracting immune cells.[4,5,7–9,14] Microarray and qPCR data (**Figure 6A**) revealed that *Ccl1*, *Ccl8*, *Cxcl9,* and *Cxcl13* were highly expressed with their receptor genes in the MRL/lpr RP; we therefore focused on them as candidates associated with UTALS development.

We next stimulated mouse mLSs composed of 87% $CD45^+$ immune cells, 8% $vimentin^+$ stromal cells, and others (**Figure 6B**) with urine *in vitro*. We used 25% urine, a concentration that stimulated the expression of cytokines/chemokines without altering *Actb* expression. Among the examined cytokines or candidate CCLs/CXCLs, healthy C57BL/6- or MRL/MpJ-derived mLSs significantly induced *Ifng*, *Tnf*, *Cxcl9*, or *Cxcl13* expression after urine administration (**Supplemental Figure 12A–C**). Notably, MRL/MpJ-derived mLSs exhibited elevated expression of these cytokines/chemokines after stimulation with MRL/lpr urine (**Figure 6C**). CXCL9 and CXCL13 tended to be strongly induced by urine from MRL/lpr compared with that from MRL/MpJ (**Supplemental Figure 12D**).

In MRL/lpr RP, *Cxcl9* and *Cxcl13* mRNA was detected in interstitial stromal cells, and $CXCL9^+$ or $CXCL13^+$ cells were positive for vimentin, a fibroblast marker (**Figure 6D, E**). In humans, $CXCL9^+$ or $CXCL13^+$ cells were scarce in the normal kidney, but several $CXCL9^+$ or $CXCL13^+$ cells showed co-localization with podoplanin (PDPN), a marker of stromal immunofibroblasts,[7] in patients with non-infectious chronic nephritis (**Figure 6F**) and infectious pyelonephritis (**Supplemental Figure 13**). Based on these results, we stimulated NIH3T3

fibroblasts with MRL/lpr-derived urine. Urine stimulation specifically induced CXCL13 expression, and increased fibroblast size and CXCL13 positivity (**Figure 6G, H**); similarly, MRL/MpJ urine also induced CXCL13 expression (**Supplemental Figure 12D**). These results indicate that the examined chemokines are expressed in UTALS-forming cells and contribute toward attracting immune cells *in situ*. Furthermore, there was a significant correlation between GL, TIL, or TLS indices and CXCL9 and CXCL13 expression in the RPs (**Table 2**).

Unique role of a collagen family in UTALS development

Given that histopathological analysis suggested a strong association between collagen fibers and UTALS development, we next focused on collagen families. STRING analysis of upregulated gene sets in mouse RP showed a cluster of several collagen genes (**Supplemental Figure 14**). Microarray analysis results of collagen genes highly expressed in the RP compared with the kidney in both mouse strains are summarized in **Figure 7A**. *Col17a1* was found highly expressed in the RPs (**Figure 7B**). COL17A1, also known as bullous pemphigoid antigen II (BP180), is expressed in the epidermis.[22] Ectopic COL17A1^{+} staining was strong in well-developed UTALSs but faint in the urothelium covering RPs that did not develop UTALSs (**Figure 7C**). Histologically, COL17A1 expression indices in the urothelium were significantly and positively correlated with those of UTALS development in MRL/lpr (**Figure 7D**). COL17A1^{+} staining was also detected in basal cells of the urothelium in human RPs with nephritis, and its staining intensity was faint in normal kidneys but stronger in infected kidneys (**Figure 7E**).

Microarray analysis revealed that immune-associated GO terms were significantly upregulated in mLSs after stimulation by rhCOL17A1 (**Supplemental Data 2, Table 3**). Predicted promoter region analysis of mouse *Col17a1* using JASPAR revealed the highest scores in the binding site of FOS or JUN—transcriptional regulators mediated by several cytokines like TNF-α. FOS and JUN localized to the nuclei of both COL17A1^{-} and COL17A1^{+} urothelium covering mouse UTALSs (**Figure 8A**). Furthermore, FOS exhibited nuclear translocation in HUCs after stimulation with urine from patients with nephritis (**Figure 8B**). TNF-α significantly increased

COL17A1, *FOS*, and *JUN* expression in HUC (**Figure 8C**).

Next, we assessed the role of COL17A1 in UTALS development by stimulating mLSs with rhCOL17A1, which increased the viability of mLS cells (**Figure 8D**). Inflammatory gene expression (*Ifng*, *Il1b, Il6*) at 3 h and IL-6 secretion at 3 and 15 h in mLSs were significantly increased post rhCOL17A1 stimulation (**Figure 8E, F**). For microarray analysis (**Supplemental Data 2**), *Cxcl9* from among the chemokine candidates as well as immune response genes (*Il22*, *Edn1*, *Cxcl2*, *Ptgs2*) were significantly upregulated after rhCOL17A1 stimulation in mLSs, indicating that they act downstream of the COL17A1-related pathway (**Figure 8G**). Notably, *Il6*, *Cxcl9*, and *Il22* expression was significantly upregulated in all examined cells separated from mLSs, $CD11b^+$ cells (APC, monocytes) and NIH3T3 fibroblasts, and $CD11b^+$ cells after 4 h of rhCOL17A1 stimulation, respectively (**Figure 8H**).

Discussion

This study demonstrated that UTALSs form in the RPs of humans and mice with chronic nephritis and revealed a mechanism of immune-related kidney lesion induction, regardless of RP-related infections. Although LSs were not clearly developed in normal human kidney RPs, reticular fiber between LSs was observed,[23] indicating that RPs may provide a scaffold for immune cells to form LSs. Furthermore, UTALS development appears to require stimulation that alters local immune microenvironments, chemotactic factor-producing cells, and immune cell entry. As shown in C57BL/6N and a previous study,[4] aging is a crucial factor for UTALS development.

Although pyelonephritis is primarily caused by UT infections,[10,24] our non-infectious, specific pathogen-free mice developed UTALS. MRL/lpr accumulate aberrant lymphocytes in systemic LSs owing to the *lpr* mutation in *Fas,* an apoptotic gene.[25] Therefore, this mutation and the subsequent inflammatory phenotype represents an established mechanism underlying LS development. In fact, a recent study using AID-prone (NZBxNZW)F1 also reported TLSs in the RPs,[4,26] and severe cell aggregations were observed in the RPs of humans with pyelonephritis.[27] In addition to AID and infection, our data suggest that urine is another unique factor contributing to UTALS formation in the RP. Nephritic urine contains bioactive molecules, including IFN-γ, TNF-α, and chemokines.[28–30] Notably, MRL/lpr urine stimulated cytokine/chemokine production in mLSs and CXCL13 in fibroblasts. Healthy C57BL/6N and MRL/MpJ urine also partially stimulated this production. Hence, the contact between RP cells and urine may play a crucial role in UTALS development via chemokine production, while changes in the abundance of urinary bioactive molecules modifies the immunological response of RP cells.

Urine leakage from the RP lumen into the parenchyma through the urothelium is required to stimulate RP cells *in vivo*. Infections or other diseases may rupture urothelial TJs, composed of OCLN or ZO-1, thereby disrupting the UB.[31] Our findings indicated that UB integrity was altered in RPs that form UTALSs, as demonstrated by the abnormal localization of TJ-associated molecules, especially decreased OCLN expression in nephritic mice. However, because altered UB integrity did not strongly induce well-developed UTALS formation as found in aged or

nephritic mice (**Supplemental Figure 10**), we considered that the altered urine condition due to renal pathology is also important for UTALS development. Notably, IFN-γ levels were increased in nephritis urine, while *OCLN* levels were decreased by IFN-γ and urine from nephritis mice, and TJ-mediated cell cluster formation was inhibited by IFN-γ in HUCs. TLS formation in the urinary bladder due to altered UB integrity has been reported previously.[14] Leakage of ovo-albumin from the epithelium to the parenchyma due to inflammation and development of dry eye and decreased OCLN expression was also reported.[32] Furthermore, pro-inflammatory cytokines reportedly alter epithelial barrier integrity in the intestinal and brain vessels.[19–21] These findings suggest a potential mechanism underlying UTALS formation, wherein altered UB integrity, caused by immune mediators from the RP and immunoreactive urine, lead to UTALS formation via leakage of urine from the RP lumen.

COL17A1 was ectopically[22] localized to the urothelium to cover the UTALS and generated immunoreactive activity. Although there is no previous record of COL17A1 function in the urothelium, GO analysis of COL17A1-stimulated mLS suggests that COL17A1 plays a role in immunological events. The FOS/JUN pathway, mediated by urinary immune mediators such as TNF-α, was also implicated in COL17A1 expression induction in the urothelium. Notably, nuclear localization of FOS/JUN was observed prior to COL17A1 expression in mouse RP urothelium. Furthermore, IL-22, which acts downstream of COL17A1, is an immunological modulator between the epithelium and parenchyma of the skin, inducing antimicrobial peptides in keratinocytes.[33] IL-22 is also elevated in patients with UT infections and nephritis.[34,35] Furthermore, our data suggest that $CD11b^+$ cells (APC, monocytes) produce IL-22 in response to COL17A1. Therefore, urine- and/or RP-derived molecules, particularly TNF-α, may activate the FOS/JUN pathway, increasing COL17A1 expression in RP parenchymal cells and subsequently inducing UTALS development via activation of downstream molecules such as IL-22.

RP stromal cells are involved in UTALS development by producing chemotactic factors. Several studies have indicated that CXCL13 is crucial for TLS development.[4,5,8,36] Previously, we also found that CXCL9- or CXCL13-expressing stromal cells in perivascular TLS formed in the

MRL/lpr kidneys.[37] CXCLs were also considered important for UTALS development, as the expression of *Cxcl9* and *Cxcl13* and their receptor genes *Cxcr3* and *Cxcr5* was elevated in mouse RPs. Stromal cells expressing these chemokines localized to mouse and human UTALS, while mouse urine stimulated CXCL13 production in mLSs and fibroblasts; and CXCL9 production in mLSs. Additionally, COL17A1 exposure increased *Cxcl9* expression in mLSs and NIH3T3 fibroblasts. CXCL9 and CXCL13 are strongly induced by IFN-γ and bind CXCR3 on either helper or effector T cells and innate-type lymphocytes as well as CXCR5 on B cells.[38,39] Specifically, $PDPN^+$ chemokine-expressing stromal immunofibroblasts,[7] including those in the human RP, are key modulators of UTALS and their phenotype is regulated by IL-22.[7] Notably, the renal parenchyma is directly connected to RPs via connective tissues composed of stromal cells. Moreover, we revealed a positive correlation between UTALS development and both TIL and TLS formation in the kidneys.

Although altered local immune conditions due to aging, infection, or AID are crucial factors for inducing the development of UTALS, we propose another pathway of pathogenesis involving RP stromal cells in UTALS development and renal pathogenesis via the connective tissue pathway resulting in either TLSs or TILs (**Supplemental Figure 15**). Specifically, bioactive factors from the urine and RP alter the UB, allowing urine leakage from the RP lumen into its parenchyma, where it immunologically stimulates RP stromal cells to produce cytokine/chemokines that attract immune cells. COL17A1 induction in the urothelium appears to be involved in these processes, and pathological crosstalk was observed between UTALSs and renal lesions stemming from TILs or TLSs. Therefore, UTALS formation caused by urine–UB alteration may represent an additional mechanism underlying the pathogenesis of chronic nephritis, regardless of infection.

Author contributions

OI, MH, TH, YO, and YK conceptualized the study design. OI designed the experiments. OI, MH, MAM, YO, and TaN performed the experiments. OI and TeN analyzed the data. MH, TH, and TaN collected the samples. MAM performed IHC and ISH. MH, MAM, TH, TeN, and YHAE reviewed and discussed the results and contributed to the preparation of the manuscript. YK supervised the project.

Acknowledgements

NIH3T3 was kindly provided by Dr. H. Yasui (Hokkaido University, Sapporo, Japan).

Data availability

The microarray data are available as **Supplemental Data 1** and **Supplemental Data 2**. The remaining data that support the findings of this study are available from the corresponding author upon reasonable request.

Disclosures

The authors declare no competing interests.

Funding

This work was supported by the Japan Society for the Promotion of Science (grant number 19K22352, 21H04751); Suzuken Memorial Foundation (grant number 18-057); Nakajima Foundation (grant number H31); and Suhara Memorial Foundation (grant number H30). The funders had no role in either the study design, data collection, analysis, decision to publish, or preparation of the manuscript.

Supplemental material table of contents

infectious pyelonephritis.

Supplemental Figure 14. Collagen family expression in the mouse RP.

Supplemental Figure 15. Formation of UTALSs in the RP is associated with alterations in the urine–urothelium barrier.

Supplemental Data 1. Summary of genes expressed in the kidney and renal pelvis of MRL/MpJ and MRL/lpr mice (microarray analysis).

Supplemental Data 2. Summary of genes expressed in the murine mimic lymphoid tissues after stimulation by human recombinant collagen type XVII alpha 1 (microarray analysis).

References

1. Pabst R: Plasticity and heterogeneity of lymphoid organs. What are the criteria to call a lymphoid organ primary, secondary or tertiary? Immunol Lett 112: 1–8, 2007
2. Pipi E, Nayar S, Gardner DH, Colafrancesco S, Smith C, Barone F: Tertiary lymphoid structures: Autoimmunity goes local. Front Immunol 9: 1952, 2018
3. Munoz-Erazo L, Rhodes JL, Marion VC, Kemp RA: Tertiary lymphoid structures in cancer – considerations for patient prognosis. Cell Mol Immunol 17: 570–575, 2020
4. Dorraji SE, Hovd A-MK, Kanapathippillai P, Bakland G, Eilertsen GØ, Figenschau SL, et al.: Mesenchymal stem cells and T cells in the formation of Tertiary Lymphoid Structures in Lupus Nephritis. Sci Rep 8: 7861, 2018
5. Sato Y, Mii A, Hamazaki Y, Fujita H, Nakata H, Masuda K, et al.: Heterogeneous fibroblasts underlie age-dependent tertiary lymphoid tissues in the kidney. JCI Insight 1: 2016
6. Chopra T, Rosner MH: Recent advances in CKD and ESRD: A literature update. Hemodial Int 21: 11–18, 2017
7. Nayar S, Campos J, Smith CG, Iannizzotto V, Gardner DH, Mourcin F, et al.: Immunofibroblasts are pivotal drivers of tertiary lymphoid structure formation and local pathology. Proc Natl Acad Sci USA 116: 13490–13497, 2019
8. He DN, Chen WL, Long KX, Zhang X, Dong GF: Association of serum CXCL13 with intrarenal ectopic lymphoid tissue formation in lupus nephritis. J Immunol Res 2016: 2016
9. Welsh-Bacic D, Lindenmeyer M, Cohen CD, Draganovici D, Mandelbaum J, Edenhofer I, et al.: Expression of the chemokine receptor CCR6 in human renal inflammation. Nephrol Dial Transplant 26: 1211–20, 2011
10. Ademola BL, Atanda AT, Aji SA, Abdu A: Clinical, morphologic and histological features of chronic pyelonephritis: An 8-year review. Niger Postgrad Med J 27: 37–41, 2020
11. Lee JH, Lee YM, Cho JH: Risk factors of septic shock in bacteremic acute pyelonephritis patients admitted to an ER. J Infect Chemother 18: 130–133, 2012

12. Obrișcă B, Jurubiță R, Andronesi A, Sorohan B, Achim C, Bobeica R, et al.: Histological predictors of renal outcome in lupus nephritis: the importance of tubulointerstitial lesions and scoring of glomerular lesions. Lupus 27: 1455–1463, 2018
13. Makino T, Miwa S, Koshida K, Kawashima A: Mucosa-associated lymphoid tissue lymphoma involving the kidney: a case report and review of the literature. Int Cancer Conf J 5: 82–89, 2016
14. Ligon MM, Wang C, Jennings Z, Schulz C, DeJong EN, Lowder JL, et al.: Tertiary lymphoid tissue develops during normal aging in mice and humans. bioRxiv 749200, 2019
15. Ichii O, Otsuka S, Sasaki N, Namiki Y, Hashimoto Y, Kon Y: Altered expression of microRNA miR-146a correlates with the development of chronic renal inflammation. Kidney Int. 81: 280–292, 2012
16. Hosotani M, Ichii O, Nakamura T, Otsuka-Kanazawa S, Hosny Y, Elewa A, et al.: Autoimmune abnormality affects ovulation and oocyte-pick-up in MRL/MpJ-Fas lpr/lpr mice. Lupus 27: 82–94, 2018
17. Yokoyama N, Ohta H, Yamazaki J, Kagawa Y, Ichii O, Khoirun N, et al.: Localization of Toll-like receptor (TLR) 2 and TLR4 mRNA in the colorectal mucosa of miniature Dachshunds with inflammatory colorectal polyps. J Comp Pathol 156: 183–190, 2017
18. Buckley AG, Looi K, Iosifidis T, Ling KM, Sutanto EN, Martinovich KM, et al.: Visualisation of multiple tight junctional complexes in human airway epithelial cells. Biol Proced Online 20: 2018
19. Rahman MT, Ghosh C, Hossain M, Linfield D, Rezaee F, Janigro D, et al.: IFN-γ IL-17A, or zonulin rapidly increase the permeability of the blood-brain and small intestinal epithelial barriers: Relevance for neuro-inflammatory diseases. Biochem Biophys Res Commun 507: 274–279, 2018
20. Sharma D, Malik A, Guy CS, Karki R, Vogel P, Kanneganti T-D: Pyrin inflammasome regulates tight junction integrity to restrict colitis and tumorigenesis. Gastroenterology 154: 948-964.e8, 2018

21. Kuo W-T, Shen L, Zuo L, Shashikanth N, Ong MLDM, Wu L, et al.: Inflammation-induced occludin downregulation limits epithelial apoptosis by suppressing caspase-3 expression. Gastroenterology 157: 1323–1337, 2019
22. Nishie W: Collagen XVII processing and blistering skin diseases. Acta Derm Venereol 100: 2020
23. Sobocinski GP, Toy K, Bobrowski WF, Shaw S, Anderson AO, Kaldjian EP: Ultrastructural localization of extracellular matrix proteins of the lymph node cortex: Evidence supporting the reticular network as a pathway for lymphocyte migration. BMC Immunol 11: 42, 2010
24. Johnson JR, Russo TA: Acute pyelonephritis in adults. N Engl J Med 378: 48–59, 2018
25. Drappa J, Brot N, Elkon KB: The Fas protein is expressed at high levels on CD4+CD8+ thymocytes and activated mature lymphocytes in normal mice but not in the lupus-prone strain, MRL lpr/lpr. Proc Natl Acad Sci USA 90: 10340–10344, 1993
26. Dorraji SE, Kanapathippillai P, Hovd AMK, Stenersrød MR, Horvei KD, Ursvik A, et al.: Kidney tertiary lymphoid structures in lupus nephritis develop into large interconnected networks and resemble lymph nodes in gene signature. Am J Pathol 190: 2203–2225, 2020
27. Sato Y, Boor P, Fukuma S, Klinkhammer BM, Haga H, Ogawa O, et al.: Developmental stages of tertiary lymphoid tissue reflect local injury and inflammation in mouse and human kidneys. Kidney Int 98: 448–463, 2020
28. Wen S, He F, Zhu X, Yuan S, Liu H, Sun L: IFN-γ, CXCL16, uPAR: Potential biomarkers for systemic lupus erythematosus. Clin Exp Rheumatol 36: 36–43, 2018
29. Moledina DG, Perry Wilson F, Pober JS, Perazella MA, Singh N, Luciano RL, et al.: Urine TNF-α and IL-9 for clinical diagnosis of acute interstitial nephritis. JCI Insight 4: 2019
30. Soliman S, Mohan C: Lupus nephritis biomarkers. Clin Immunol 185: 10–20, 2017
31. Lee JD, Lee MH: Decreased expression of zonula occludens-1 and occludin in the bladder urothelium of patients with interstitial cystitis/painful bladder syndrome. J Formos Med Assoc 113: 17–22, 2014

32. Bian F, Xiao Y, Barbosa FL, de Souza RG, Hernandez H, Yu Z, et al.: Age-associated antigen-presenting cell alterations promote dry-eye inducing Th1 cells. Mucosal Immunol 12: 897–908, 2019

33. Sonnenberg GF, Fouser LA, Artis D: Border patrol: regulation of immunity, inflammation and tissue homeostasis at barrier surfaces by IL-22. Nat Immunol 12: 383–90, 2011

34. Ahmadikia K, Kordbacheh P, Shadpour P, Nami S, Sarrafnejad A, Mahmoodi M, et al.: Increased urine interleukin-17 and interleukin-22 levels in patients with candidal urinary tract infection. Iran J Kidney Dis 12: 33–39, 2018

35. Yang X, Weng Q, Hu L, Yang L, Wang X, Xiang X, et al.: Increased interleukin-22 levels in lupus nephritis and its associated with disease severity: a study in both patients and lupus-like mice model. Clin Exp Rheumatol 37: 400–407

36. Fleige H, Ravens S, Moschovakis GL, Bölter J, Willenzon S, Sutter G, et al.: IL-17-induced CXCL12 recruits B cells and induces follicle formation in BALT in the absence of differentiated FDCs. J Exp Med 211: 643–651, 2014

37. Masum MA, Ichii O, Elewa YHA, Otani Y, Namba T, Kon Y: Vasculature-associated lymphoid tissue: a unique tertiary lymphoid tissue correlates with renal lesions in lupus nephritis mouse model. Front Immunol 11: 3211, 2020

38. Groom JR, Luster AD: CXCR3 ligands: redundant, collaborative and antagonistic functions. Immunol Cell Biol 89: 207–215, 2011

39. Rao DA: T cells that help B cells in chronically inflamed tissues. Front Immunol 9: 1924, 2018

Table 1. Correlation between UTALS development indices (immune cell markers) and pathological parameters in mice.

Disease parameter		Indices for UTALS development (expression in RP)		
		Immune cell marker		
Category	**Parameter**	**CD25 (*Il2ra*)**	**CD3 (*Cd3e*)**	**B220 (*Ptprc*)**
GL	Glomerular area	0.679**	0.779**	0.718**
	$CD3^+$ cell density	0.685**	0.681**	0.715**
	$B220^+$ cell density	0.774**	0.769**	0.737**
TIL	$CD3^+$ score	0.684**	0.765**	0.787**
	$B220^+$ score	0.755**	0.801**	0.699**
TLS	% of $CD3^+$ cluster	0.713**	0.848**	0.850**
	% of $B220^+$ cluster	0.703**	0.873**	0.860**

Value = ρ (Spearman's rank correlation coefficient). MRL/MpJ (n = 7), MRL/lpr (n = 10). $^{**}P$ <0.01; $^{*}P$ <0.05. mRNA expression was normalized to that of *Actb*. GL, glomerular lesion; TIL, tubulointerstitial lesion; TLS, tertiary lymphoid structure; UTALS, urinary tract-associated lymphoid structure.

Table 2. Correlation between UTALS development indices (chemokines) and pathological parameters in mice.

Disease parameter		Indices for UTALS development (expression in RP)	
		Chemokine	
Category	**Parameter**	***Cxcl9***	***Cxcl13***
GL	Glomerular area	0.504	0.688**
	$CD3^+$ cell density	0.757**	0.696**
	$B220^+$ cell density	0.747**	0.623*
TIL	$CD3^+$ score	0.639*	0.738**
	$B220^+$ score	0.489	0.509*
TLS	% of $CD3^+$ cluster	0.650**	0.629**
	% of $B220^+$ cluster	0.486	0.591*

Value = ρ (Spearman's rank correlation coefficient). MRL/MpJ (n = 7), MRL/lpr (n = 10). $^{**}P$ <0.01; $^{*}P$ <0.05. mRNA expression was normalized to that of *Actb*. GL, glomerular lesion; TIL, tubulointerstitial lesion; TLS, tertiary lymphoid structure; UTALS, urinary tract-associated lymphoid structure.

Table 3. Gene ontology of mLS cells after stimulation with rhCOL17A1.

Pathway GO ID	Pathway description	Gene count	FDR
0006952	Defense response	88	3.46E-39
0002376	Immune system process	99	2.76E-33
0006955	Immune response	75	4.18E-33
0051707	Response to other organism	79	8.53E-33
0034097	Response to cytokine	69	6.08E-32
0006954	Inflammatory response	54	1.82E-30
0009605	Response to external stimulus	102	3.59E-30
0071345	Cellular response to cytokine stimulus	61	9.88E-29
0050896	Response to stimulus	183	2.25E-27
0006950	Response to stress	114	3.20E-25

Ten upregulated GO terms are listed. Stimulation with 0.4 μg/mL rhCOL17A1 for 4 h; microarray. GO, gene ontology.

Figure legends

Figure 1. RP histopathology in human patients with infectious or non-infectious nephritis.

(A and B) Histopathology of the human kidney (A) and RP (B). Patients with pyelonephritis and chronic nephritis show severe glomerular lesions and tubulointerstitial lesions (A) and cell infiltrations in the RP regardless of infection (B). Insets indicate the magnified square area. Lu, lumen of RP; RP, renal pelvis; Masson's trichrome (MT) staining.

(C–E) Localization of $CD3^+$ T cells (C), $COL3A1^+$ fibers (D), and $PNAd^+$ high endothelial venules (HEVs) (E) in the RP of normal kidney donors and patients with nephritis. Numerous $CD3^+$ cells are localized in the lamina propria and urothelium in both patients (C). Strong $COL3A1^+$ reactions are observed in all RP samples (D). Arrows show $PNAd^+$ HEVs, and insets indicate the magnified square area (D, E); immunohistochemistry.

Normal: female, 33 years. Pyelonephritis: male, 39 years. Chronic nephritis: male, 69 years.

(F and G) Histopathology of the human kidney (F) and RP (G) in different samples of A–E. Necropsy samples of human kidneys showing normal histopathology and moderate or severe tubulointerstitial cell infiltration in non-infectious chronic nephritis. Normal kidney exhibited scarce cell infiltrations in both the tubulointerstitium and RP. In the kidney showing moderate cell infiltration, mononuclear cells are scattered in the RP parenchyma beneath the urothelium. In the kidney showing severe lesions, severe cell infiltrations are also observed in RP; MT staining.

Normal: female, 34 years. Moderate: male, 52 years. Severe: male, 53 years.

Scale bars = 50 μm (A and F), 100 μm (B–E, and G).

Figure 2. Localization and cell composition of UTALSs in the mouse kidney.

C57BL/6N (6 months) were used in panels B–F. C57BL/6N and B6.MRLc1 (9 months) were used in G and H.

(A) UTALS localization considering RP morphology. Dotted straight lines indicate distance from the reference section (0 μm) at approximately 500 μm intervals. Red circles; UTALS.

(B) Immune cell marker gene expression in the kidney and RP. aT, active T cells; aB, active B

cells; Mφ, macrophages; panT, pan T cells; APC, antigen-presenting cells; qPCR.

(C) Representative histological features of UTALS. Numerous cells infiltrate between connective fibers in RP; MT staining.

(D) Large UTALS comprising $CD3^+$ T cells, $B220^+$ B cells, and $IBA1^+$ macrophages. Hoechst, nuclear staining; immunofluorescence.

(E) Large UTALS comprising $COL3A1^+$ reticular fibers. Dotted line indicates the border between Lu and urothelium; immunohistochemistry.

(F) Large UTALS comprising $PNAd^+$ high endothelial venules. Insets indicate the magnified square area (right panel); immunohistochemistry.

(G) UTALS in a spontaneous mouse model for chronic glomerulonephritis. Compared with C57BL/6N, B6.MRLc1 develops UTALSs with $CD3^+$ T cells or $B220^+$ B cells in the RP and manifests glomerulonephritis in CO. $B220^+$ B cells are also observed in the urothelium (square and inset); periodic acid Schiff (PAS) staining or immunohistochemistry.

(H) $CD3^+$ T cell or $B220^+$ B cell number in the examined RP area; histoplanimetry.

Values are presented as the mean ± SE; $n = 7$ (B); $n = 7$ or 22 (C57BL/6N or B6.MRLc1) (H). Significant differences between kidney and RP or C57BL/6N and B6.MRLc1 are indicated by $^{**}P < 0.01$; Mann–Whitney *U*-test.

Scale bars = 50 μm (C, D), 10 μm (E), 100 μm (F, G). IM, inner medulla; OM, outer medulla; CO, cortex; Lu, lumen of RP; RP, renal pelvis; UE, urothelium.

Figure 3. Development of UTALSs in nephritis models.

MRL/MpJ and MRL/lpr (6 months) were used.

(A) RP histopathology, including UTALSs and the renal cortex. UTALS is well-developed in MRL/lpr than in MRL/MpJ. MRL/lpr kidney showing severe glomerular lesions and tubulointerstitial lesions; MT staining.

(B, C) Localization of $B220^+$ B cells and $CD3^+$ T cells in the RP and kidneys of MRL/MpJ (B) and MRL/lpr (C). MRL/lpr showing developed UTALSs with numerous positive cells in the RP and

renal inflammation (C). Arrows and arrowheads indicate positive cells in the glomerulus and tubulointerstitial regions, respectively; immunohistochemistry.

(D) Localization of IBA1$^+$ macrophages, MHCII$^+$ antigen-presenting cells, LYVE1$^+$ lymphatic vessels, and PNAd$^+$ high endothelial venules in MRL/lpr UTALSs. Insets indicate the magnified square area. PNAd$^+$ HEVs localization with RP (upper panel) and urothelium (lower panel); immunohistochemistry.

(E) Immune cell marker gene expression in the kidney and RP; qPCR.

Values represent the mean ± SE; n = 7 or 10 (MRL/MpJ or MRL/lpr). Significant differences between kidney and RP or MRL/MpJ and MRL/lpr are indicated by $^{\#}P$ <0.05, $^{\#\#}P$ <0.01, or $^{**}P$ <0.01; Mann–Whitney U-test.

Scale bars = 100 μm (A, RP; D, PNAd), 50 μm (A, cortex; B, C), 300 μm (D, IBA1, MHCII, LYVE1). IM, inner medulla; Lu, lumen of the RP; RP, renal pelvis.

Figure 4. Altered urothelium barrier integrity in the RPs of mice and human with nephritis.

MRL/MpJ and MRL/lpr (6 months) were used in A–E, G, and H.

(A, B) Surface ultrastructure of the RP in MRL/MpJ (A) and MRL/lpr (B). Arrowheads indicate RP walls and arrows indicate lack of urothelium in MRL/lpr mice. Dotted lines indicate the cutting surface of renal papilla; scanning electron microscopy (SEM).

(C) Surface ultrastructure of the MRL/lpr RP. Well-formed (arrows) or distorted (arrowheads) spherical cells are observed in some parts of the urothelium (left panel), a large area of the urothelium is lacking (middle panel), and alterations to the domed shape are observed (right panel); SEM.

(D) *Upk3a* and tight junction (TJ)-associated molecule gene expression, and expression of TJ-associated molecules normalized to *Upk3a* (urothelium marker) in the RP; qPCR.

(E and F) TJ-associated molecule localization in the RP of mice (E) and humans (F). Arrows indicate the faint area of OCLN$^+$ reaction, and arrowheads indicate invagination of the urothelium (E). The square and its insets indicate the urothelium. Dotted lines indicate the border between

the urothelium and RP parenchyma. Localization patterns of ZO-1$^+$ or OCLN$^+$ reactions are altered in the urothelium of both patients (F); immunofluorescence.

(G) Localization of Evans blue-conjugated bovine serum albumin (EBA; red stain). Asterisks indicate the area of the urothelium from which EBA leaked into the RP parenchyma in MRL/lpr; fluorescence microscopy.

(H) Quantification of EBA leakage in RP; histoplanimetry.

Values are shown as the mean ± SE (D and H). *n* = 7 or 10 (MRL/MpJ or MRL/lpr) (D); *n* = 7 (H). ***P* <0.01; Mann–Whitney *U*-test.

Scale bars = 500 μm (A, B, low magnification), 20 μm (A, B, high magnification; C), 50 μm (E–G). BV, blood vessels; RP, renal pelvis; IM, inner medulla; Lu, lumen of RP; CO, cortex.

Figure 5. Effect of cytokines on the urothelium barrier integrity in cultured human urothelial cells (HUCs).

(A) Determination of cytokine levels in human urine. HC, healthy control. Nephritis, non-infectious chronic nephritis; immunoassay.

(B) Receptor gene expression for TNF-α and IFN-γ in HUCs. THP1 monocytes were used as positive control. M, size marker; RT-PCR.

(C) mRNA expression of *TJP1* (gene encoding ZO-1) and *OCLN* in cultured HUCs after cytokine stimulation for 24 h; qPCR.

(D) mRNA expression of *TJP1* and *OCLN* in cultured HUCs after cytokine stimulation from pooled urine from panel A for 3 h; qPCR.

(E) TJ-associated molecules in cultured HUCs after IFN-γ stimulation for 24 h. Inset indicates the magnified square area; immunofluorescence.

(F) ZO-1$^+$OCLN$^+$ cluster size and number in cultured HUCs after IFN-γ stimulation for 24 h; morphometry.

Values are expressed as the mean ± SE (A, C, D, and F). *n* = 9 or 12 (HC or nephritis) (A); *n* = 4 (C and D); 20 area (F). **P* <0.05; ***P* <0.01; Mann–Whitney *U*-test (A, D, and F). Significant

differences compared with the PBS control (Cont) are indicated by *P <0.05; Dunnett's test (C).
Scale bars = 50 μm (E).

Figure 6. Chemokine-expressing cells in the RPs of mice and humans with nephritis and cytokine/chemokine induction in cultured cells by urine stimulation.

MRL/MpJ and MRL/lpr (6 months) were used in A–E.

(A) Gene expression of chemokine ligands or their receptors in the kidney and RP; qPCR.

(B) Percentage of $CD45^+$ immune cells and $vimentin^+$ stromal cells in MRL/MpJ-derived mimic lymphoid tissues (mLSs); immunofluorescence.

(C) Culture supernatant levels and gene expression of cytokines and chemokines in MRL/MpJ-derived mLSs after stimulation with 25% MRL/lpr urine for 4 h; ELISA and qPCR.

(D) Localization of chemokine-expressing cells in the MRL/lpr RP. Insets indicate the magnified square area; *in situ* hybridization.

(E, F) Localization of chemokines, $vimentin^+$ stromal cells, and $B220^+$ B cells in the MRL/lpr RP (E) or that of chemokines and $PDPN^+$ stromal cells in the RP of the normal human kidney and kidneys of patients with non-infectious chronic nephritis (F). Yellow arrows indicate co-localization of chemokines with vimentin or PDPN. Insets indicate the magnified square area. White dots indicate the border between the urothelium and RP parenchyma; immunofluorescence.

(G) Gene expression of cytokines and chemokines in NIH3T3 fibroblasts after stimulation with 25% urine from MRL/lpr for 4 h; qPCR.

(H) Culture supernatant CXCL13 levels and CXCL13 and vimentin expression in NIH3T3 fibroblasts after 25% MRL/lpr urine stimulation for 4 h; ELISA and immunofluorescence.

Values are expressed as the mean ± SE; n = 7 or 10 (MRL/MpJ or MRL/lpr, A), n = 4 (C, G, H). Significant differences between kidneys and RP or MRL/MpJ and MRL/lpr are indicated by $^{\#}P$ <0.05 and $^{\#\#}P$ <0.01 or *P <0.05 and **P <0.01. Significant differences compared with the PBS control (Cont) are indicated by *P <0.05 and **P <0.01; Mann–Whitney U-test.

Scale bars = 10 μm (B, H), 100 μm (D), 50 μm (E, F). Lu, lumen of RP; RP, renal pelvis.

Figure 7. COL17A1 associated with UTALS development.

MRL/MpJ and MRL/lpr (6 months) were used in A–D.

(A) Collagen family relative gene expression in the RP and kidney; microarray.

(B) *Col17a1* expression in the kidney and RP; qPCR.

(C) COL17A1 localization in the RP. COL17A1^{+} reactions are observed in the urothelium covering mature UTALSs (arrows), but not immature urinary UTALSs (asterisks). Insets: magnified square area; immunohistochemistry.

(D) Histopathological correlations of COL17A1 expression indices (X axis) in the urothelium with UTALS development indices including its nuclear number (Y axis, upper panel) or area ratio of COL17A1^{+} reactions to UTALS (Y axis, lower panel) in MRL/lpr. IntDen, integrated density; histoplanimetry.

(E) Localization of COL17A1 in the human RP. COL17A1^{+} reactions are only observed in the patient urothelium; immunohistochemistry.

Values are shown as the mean ± SE (B); n = 7 or 10 (MRL/MpJ or MRL/lpr). $^{**}P$ <0.01; Mann–Whitney U-test. $^{**}P$ <0.01; Spearman's correlation test (D).

Bars = 500 μm (C), 100 μm (E). Lu, lumen of RP; RP, renal pelvis.

Figure 8. Upstream and downstream events of COL17A1 in UTALS development.

MRL/MpJ and MRL/lpr (6 months) were used in A. C57BL/6N (6 months) mice were used in D–H.

(A) Localization of FOS, JUN, and COL17A1 in the RP. Nuclear localization of FOS and JUN (arrows) is observed in small and large UTALSs covering COL17A1^{-} and COL17A1^{+} urothelium in MRL/lpr. Lu, lumen of RP; RP, renal pelvis; immunofluorescence.

(B) Nuclear translocation of FOS after 24 h treatment with 25% human urine in HUCs; immunofluorescence.

(C) *COL17A1*, *FOS*, and *JUN* expression after 24 h treatment with 1.0 ng TNF-α in HUCs; qPCR.

(D–F) Assessment of cell viability (D), gene expression (E), and IL-6 supernatant level (F) of mLS

cells after 24 h (D) and 3 or 15 h of treatment (E and F) with bovine serum albumin (BSA) or rhCOL17A1; MTT assay (D); qPCR (E); ELISA (F).

(G) Chemokine or upregulated gene expression in mLT cells after stimulation with 0.4 μg/mL rhCOL17A1 for 4 h. Candidate chemokines or the top four upregulated genes are listed; microarray.

(H) *Il6*, *Cxcl9*, and *Il22* expression in B, T, and $CD11b^+$ cells isolated from mLSs, and NIH3T3 fibroblasts after stimulation with 0.4 μg/mL rhCOL17A1 for 4 h; qPCR.

Values are shown as the mean ± SE (C–F, H); $n = 4$ (C–E, H); $n = 4–7$ (F); $n = 3$ (G). Significant differences compared with the PBS control (Cont; C, G) or BSA (D–F, H) are indicated by $*P < 0.05$ or $**P < 0.01$; Mann–Whitney *U*-test (C, D, H), Dunnett's test (E, F), or Student's *t*-test (H). Scale bars = 50 μm (A and B).

Significance Statement

Tertiary lymphoid structures (TLSs) form in organs exhibiting chronic inflammation. Immune responses to infections, autoimmune responses, or allergic responses may trigger TLS development. Here, urine–urothelium barrier alterations were observed in the renal pelvis (RP) of a mouse model and human subjects with chronic nephritis. Furthermore, urine leakage from the RP lumen into the parenchyma was demonstrated in nephritic mice. Leaked urine stimulated the production of cytokines/chemokines in RP stromal cells, resulting in TLS development termed “urinary tract-associated lymphoid structures” (UTALSs). UTALS development was correlated with chronic nephritis development in humans and mice, regardless of urinary tract infection, and may thus be considered a novel pathological mechanism. Elucidation of this mechanism is crucial for a better understanding of non-infectious chronic nephritis.

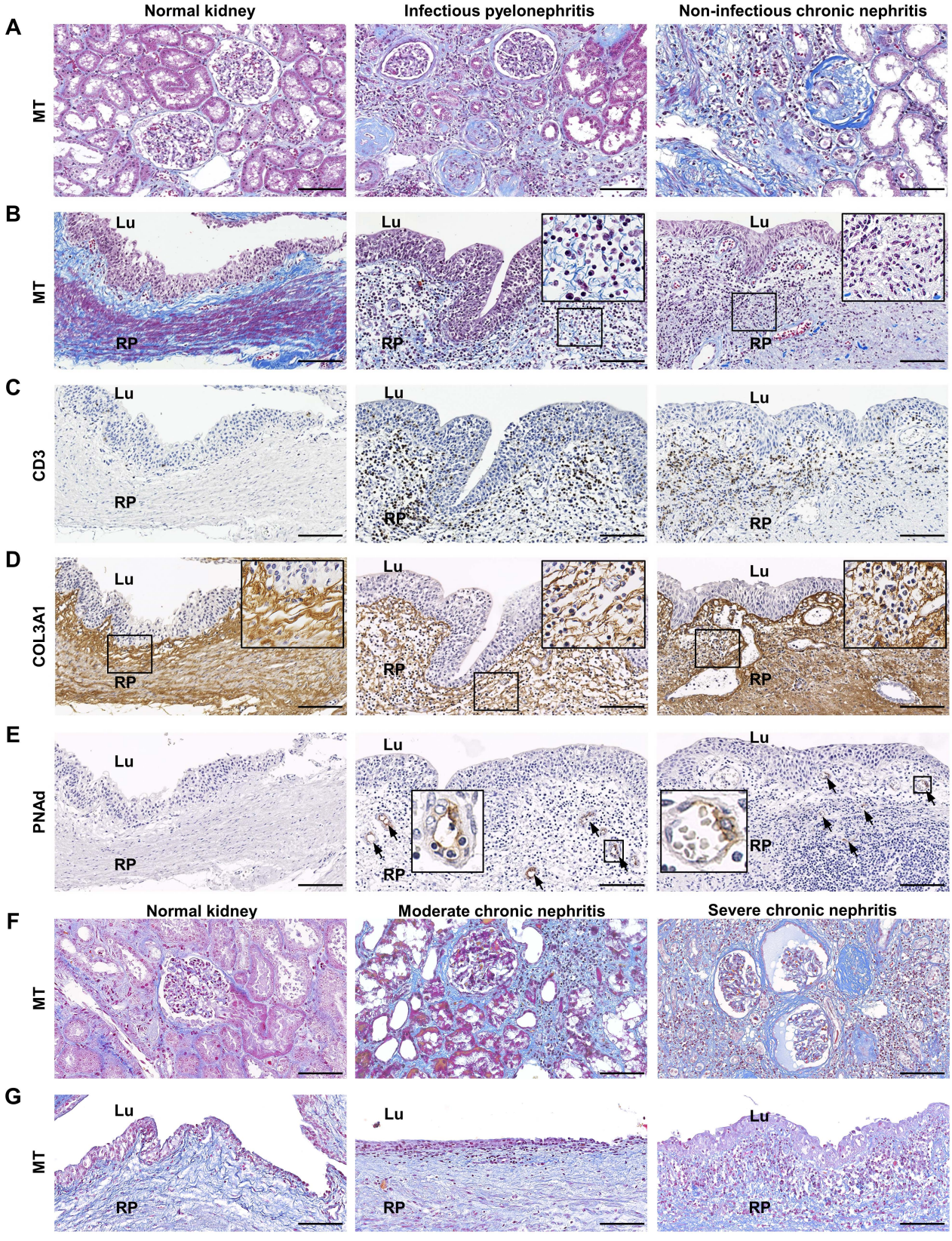
Normal kidney
Infectious pyelonephritis
Non-infectious chronic nephritis
A
MT
B
MT
Lu
RP
C
CD3
Lu
RP
D
COL3A1
Lu
RP
E
PNAd
Lu
RP
Normal kidney
Moderate chronic nephritis
Severe chronic nephritis
F
MT
G
MT
Lu
RP

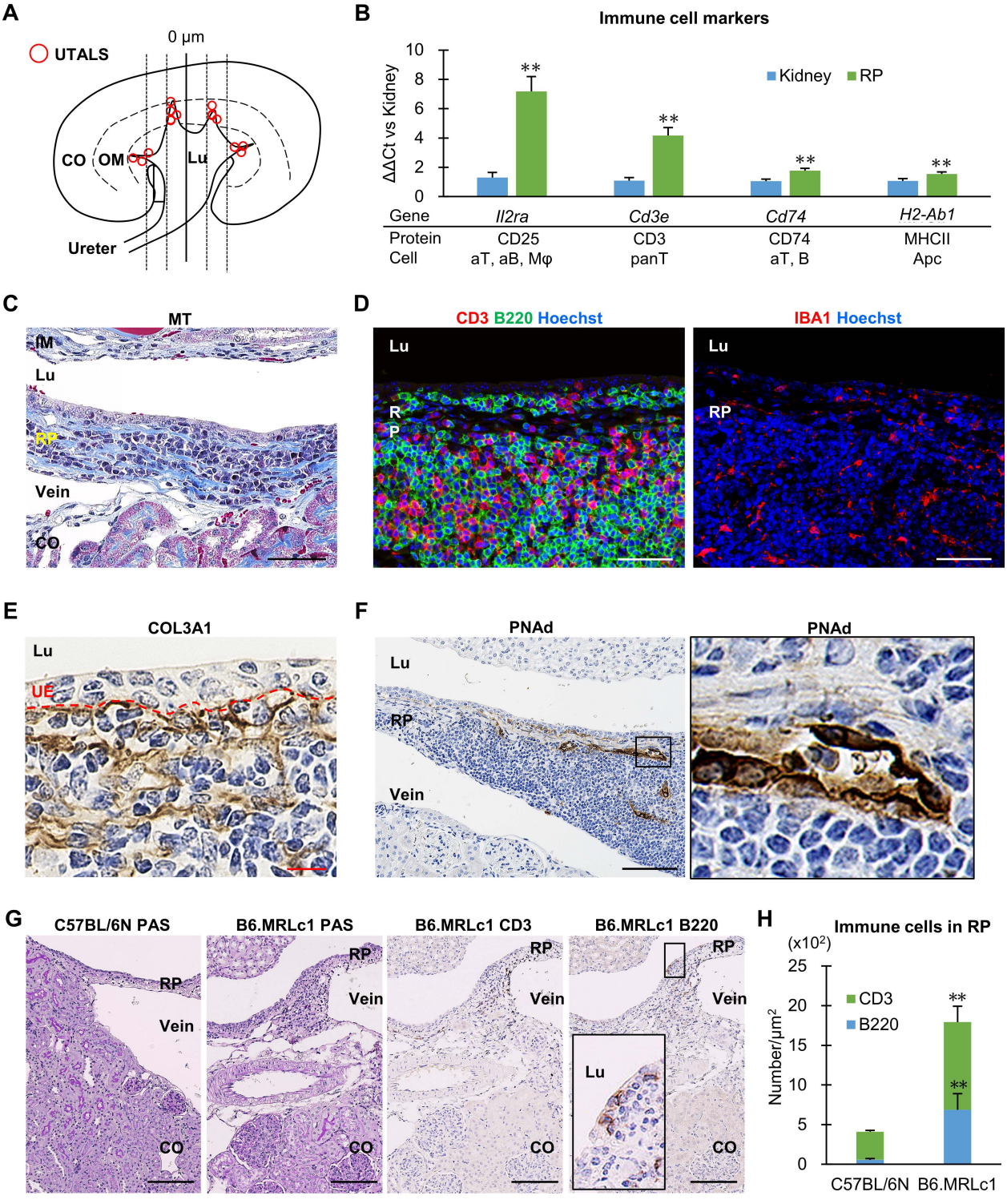
A
UTALS
0 μm
CO
OM
Lu
Ureter
B
Immune cell markers
ΔΔCt vs Kidney
Kidney
RP
Gene
Il2ra
Cd3e
Cd74
H2-Ab1
Protein
CD25
CD3
CD74
MHCII
Cell
aT, aB, Mφ
panT
aT, B
Apc
C
MT
IM
Lu
RP
Vein
CO
D
CD3 B220 Hoechst
IBA1 Hoechst
Lu
R
P
RP
E
COL3A1
Lu
UE
F
PNAd
PNAd
Lu
RP
Vein
G
C57BL/6N PAS
B6.MRLc1 PAS
B6.MRLc1 CD3
B6.MRLc1 B220
RP
Vein
CO
Lu
H
Immune cells in RP
(x10²)
Number/μm²
CD3
B220
C57BL/6N
B6.MRLc1

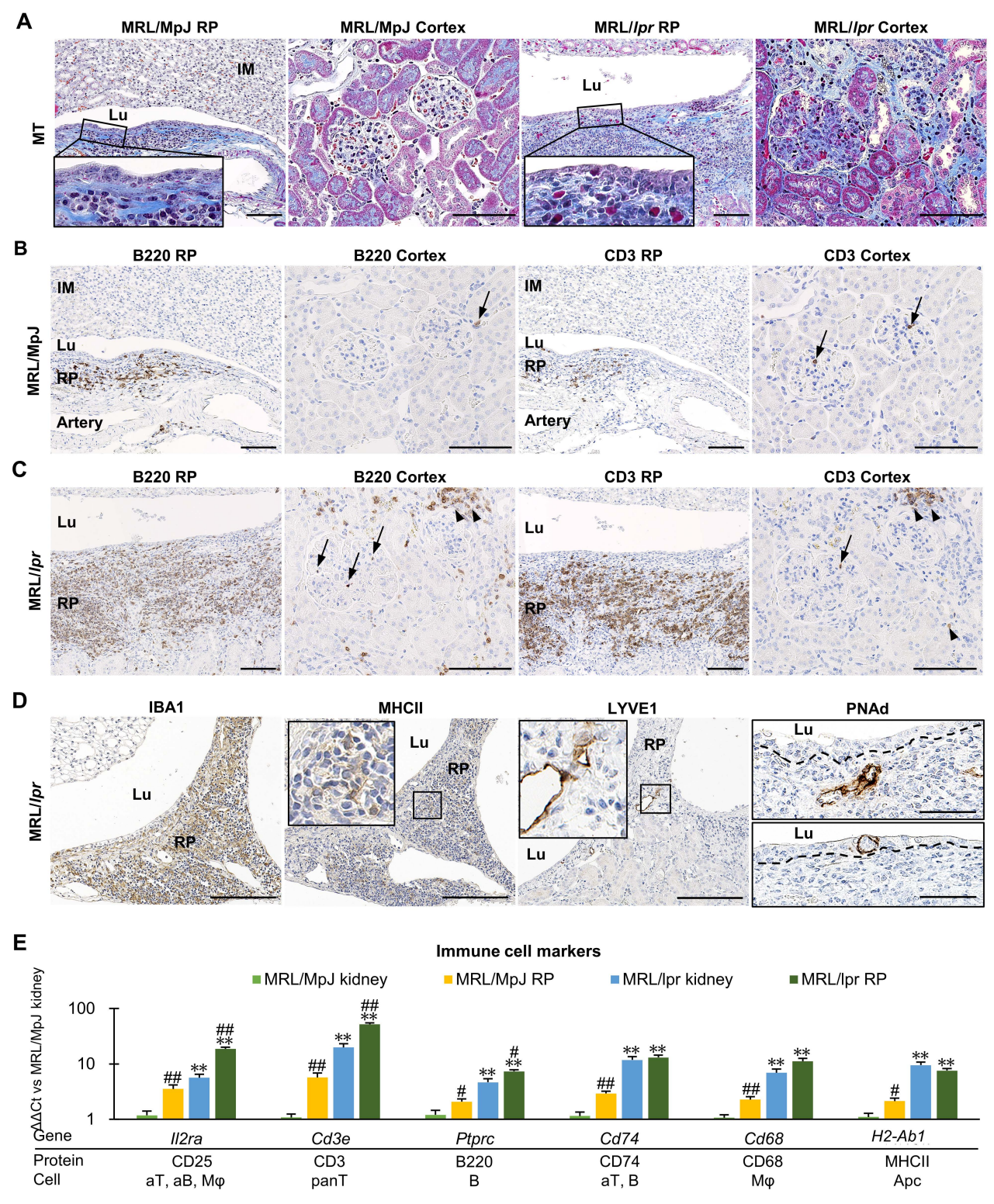
A
MRL/MpJ RP
MRL/MpJ Cortex
MRL/lpr RP
MRL/lpr Cortex
MT
IM
Lu
B
B220 RP
B220 Cortex
CD3 RP
CD3 Cortex
MRL/MpJ
IM
Lu
RP
Artery
C
MRL/lpr
Lu
RP
D
IBA1
MHCII
LYVE1
PNAd
E
Immune cell markers
MRL/MpJ kidney
MRL/MpJ RP
MRL/lpr kidney
MRL/lpr RP
ΔΔCt vs MRL/MpJ kidney
100
10
1
Gene
Il2ra
Cd3e
Ptprc
Cd74
Cd68
H2-Ab1
Protein
CD25
CD3
B220
CD74
CD68
MHCII
Cell
aT, aB, Mφ
panT
B
aT, B
Mφ
Apc

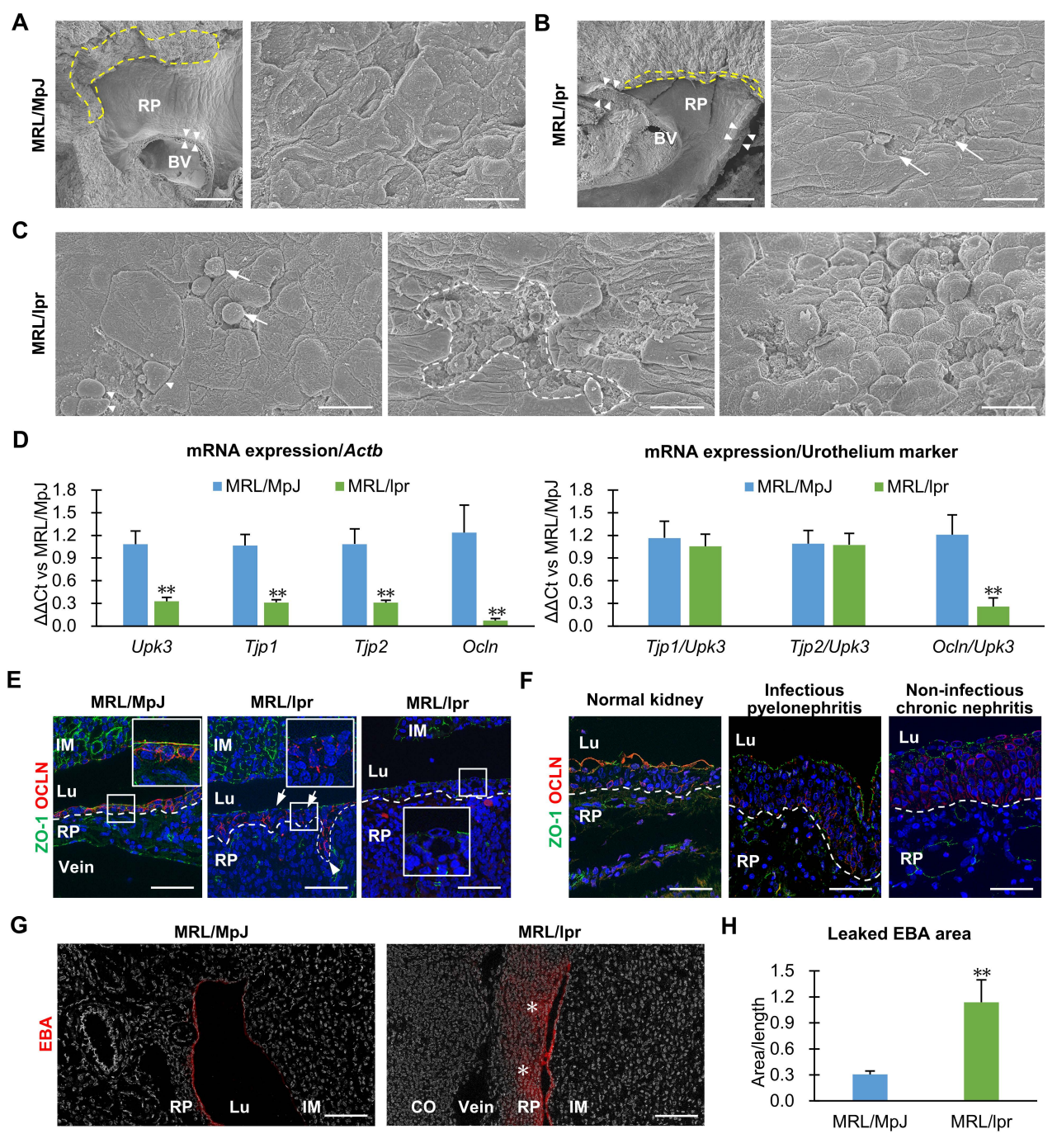
A
MRL/MpJ
RP
BV
B
MRL/lpr
RP
BV
C
MRL/lpr
D
mRNA expression/Actb
MRL/MpJ
MRL/lpr
ΔΔCt vs MRL/MpJ
1.8
1.5
1.2
0.9
0.6
0.3
0.0
**
Upk3
Tjp1
Tjp2
Ocln
mRNA expression/Urothelium marker
MRL/MpJ
MRL/lpr
ΔΔCt vs MRL/MpJ
**
Tjp1/Upk3
Tjp2/Upk3
Ocln/Upk3
E
MRL/MpJ
MRL/lpr
MRL/lpr
ZO-1 OCLN
IM
Lu
RP
Vein
F
Normal kidney
Infectious pyelonephritis
Non-infectious chronic nephritis
ZO-1 OCLN
Lu
RP
G
MRL/MpJ
MRL/lpr
EBA
RP
Lu
IM
CO
Vein
H
Leaked EBA area
Area/length
1.5
1.2
0.9
0.6
0.3
0.0
**
MRL/MpJ
MRL/lpr

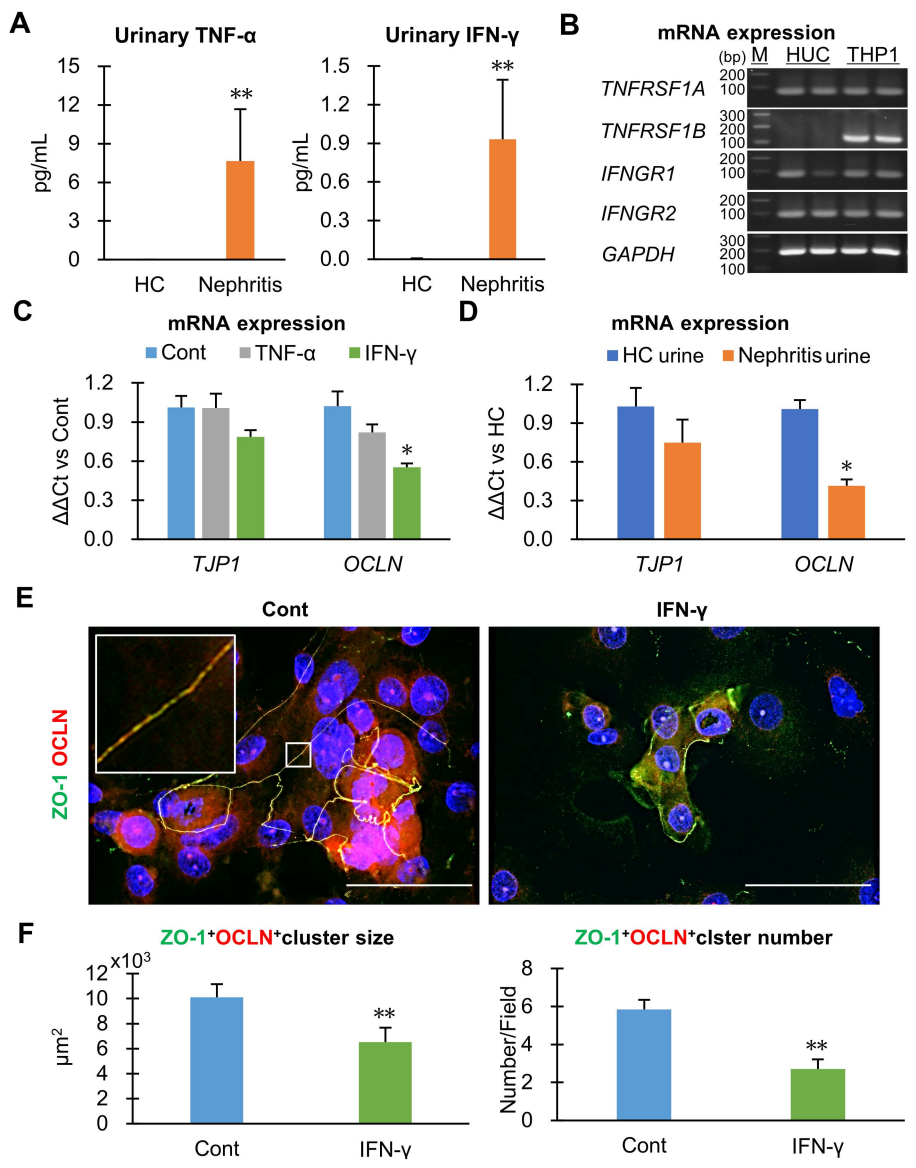
A
Urinary TNF-α
pg/mL
15
12
9
6
3
0
**
HC
Nephritis
Urinary IFN-γ
pg/mL
1.5
1.2
0.9
0.6
0.3
0.0
**
HC
Nephritis
B
mRNA expression
(bp) M HUC THP1
TNFRSF1A
TNFRSF1B
IFNGR1
IFNGR2
GAPDH
200
100
300
200
100
C
mRNA expression
Cont
TNF-α
IFN-γ
ΔΔCt vs Cont
1.2
0.9
0.6
0.3
0.0
*
TJP1
OCLN
D
mRNA expression
HC urine
Nephritis urine
ΔΔCt vs HC
1.2
0.9
0.6
0.3
0.0
*
TJP1
OCLN
E
Cont
IFN-γ
ZO-1 OCLN
F
ZO-1+OCLN+cluster size
x10^3
μm2
12
10
8
6
4
2
0
**
Cont
IFN-γ
ZO-1+OCLN+clster number
Number/Field
8
6
4
2
0
**
Cont
IFN-γ

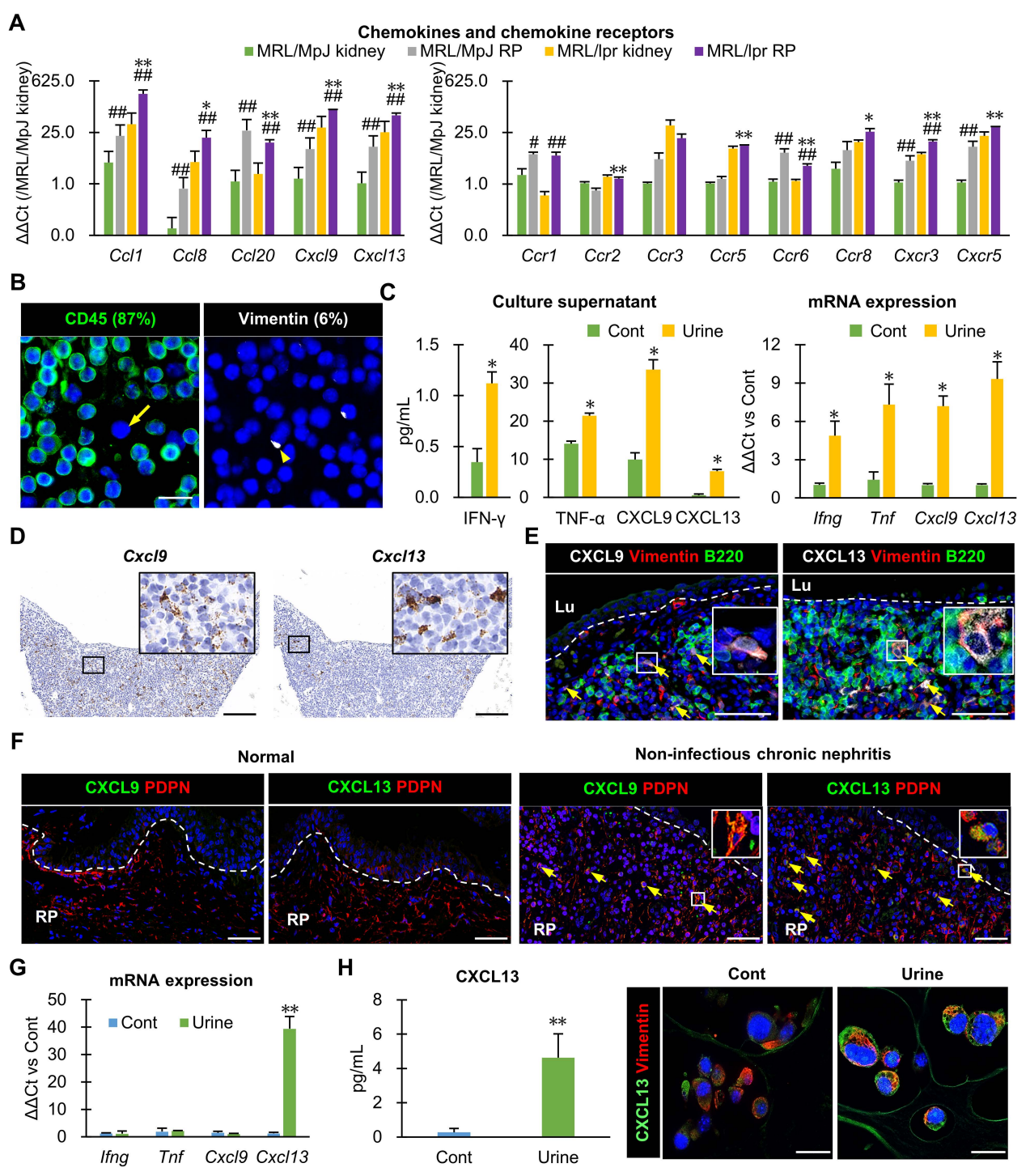
A
Chemokines and chemokine receptors
MRL/MpJ kidney
MRL/MpJ RP
MRL/lpr kidney
MRL/lpr RP
ΔΔCt (/MRL/MpJ kidney)
625.0
25.0
1.0
0.0
Ccl1
Ccl8
Ccl20
Cxcl9
Cxcl13
Ccr1
Ccr2
Ccr3
Ccr5
Ccr6
Ccr8
Cxcr3
Cxcr5
B
CD45 (87%)
Vimentin (6%)
C
Culture supernatant
Cont
Urine
pg/mL
IFN-γ
TNF-α
CXCL9
CXCL13
mRNA expression
ΔΔCt vs Cont
Ifng
Tnf
Cxcl9
Cxcl13
D
Cxcl9
Cxcl13
E
CXCL9 Vimentin B220
CXCL13 Vimentin B220
Lu
F
Normal
Non-infectious chronic nephritis
CXCL9 PDPN
CXCL13 PDPN
RP
G
mRNA expression
Cont
Urine
ΔΔCt vs Cont
Ifng
Tnf
Cxcl9
Cxcl13
H
CXCL13
pg/mL
Cont
Urine
Cont
Urine
CXCL13 Vimentin

A

	Rank	Symbol	RP/Kidney ratio MRL/MpJ	RP/Kidney ratio MRL/lpr
Collagen family	1	*Col17a1*	8.9	10.0
	2	*Col25a1*	7.4	0.7
	3	*Col4a6*	4.7	1.5
	4	*Col22a1*	3.2	0.9
	5	*Col12a1*	3.0	1.8
	6	*Col1a1*	2.9	1.6
	7	*Col23a1*	2.8	1.9
	8	*Col6a6*	2.7	0.5
	9	*Col15a1*	2.5	1.1
	10	*Col9a3*	2.3	0.7

B

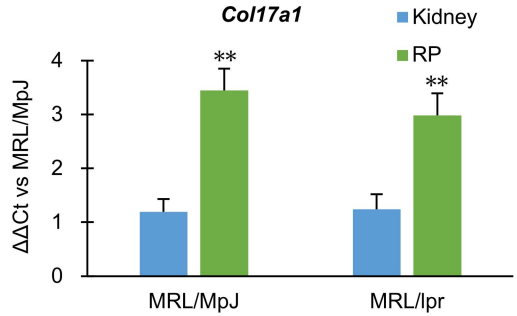

C

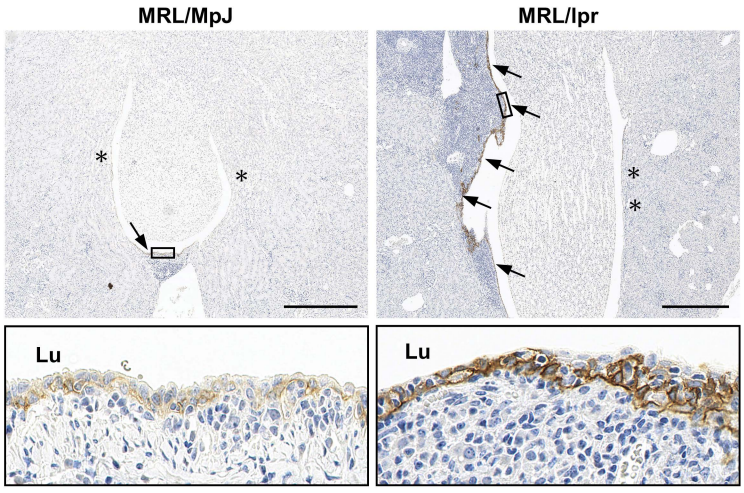

D

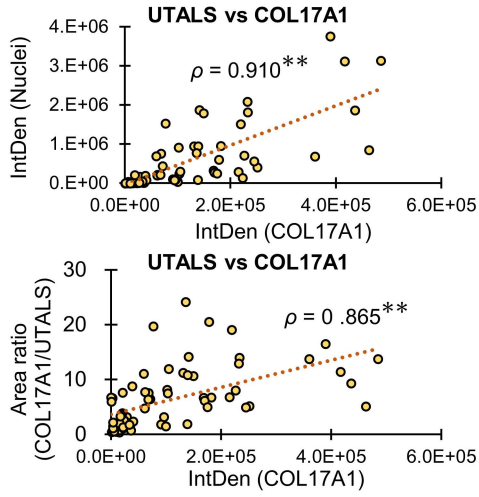

E

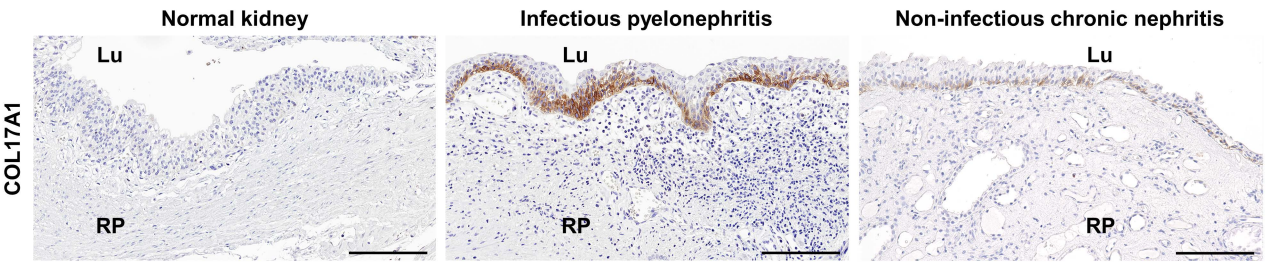

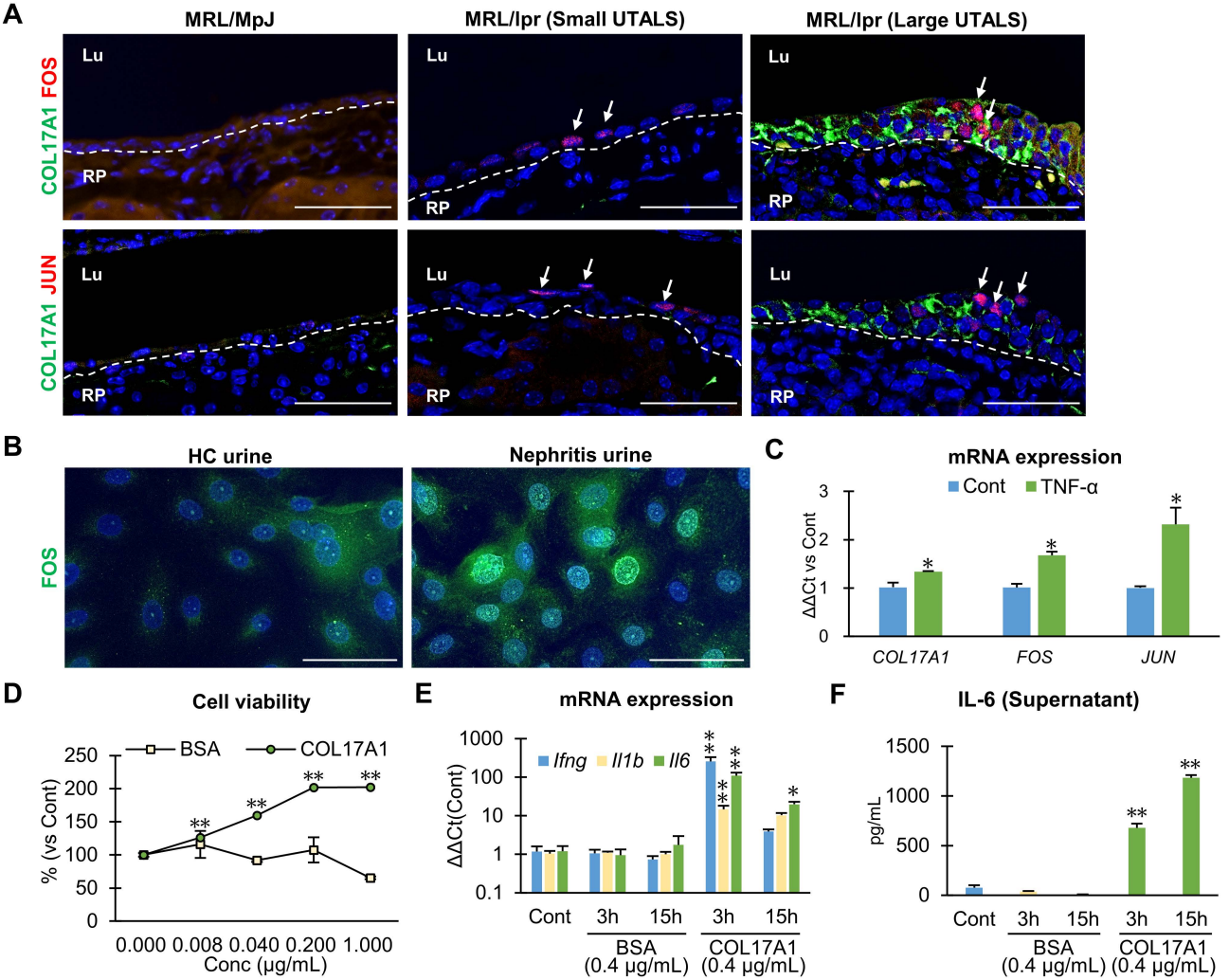

G

Chemokine		Cont			COL17A1				Top 4 genes		Cont			COL17A1			
Rank	Symbol	#1	#2	#3	#1	#2	#3	*P value*	Rank	Symbol	#1	#2	#3	#1	#2	#3	*P value*
1	*Cxcl9*	1.1	1.0	0.9	7.8	6.9	6.3	0.00018	1	*Il22*	0.7	0.7	1.6	359.4	360.4	363.1	< 0.00001
2	*Ccl1*	1.0	1.0	1.0	1.6	1.8	1.8	0.00024	2	*Edn1*	0.7	0.7	1.6	339.0	357.0	324.7	< 0.00001
3	*Ccl8*	1.0	0.9	1.1	0.8	0.7	0.6	0.01149	3	*Cxcl2*	1.0	0.5	1.5	208.7	208.3	169.6	0.00011
4	*Cxcl13*	0.7	0.7	1.6	1.2	1.8	1.0	0.45273	4	*Ptgs2*	1.0	1.0	1.0	158.0	168.6	162.1	< 0.00001

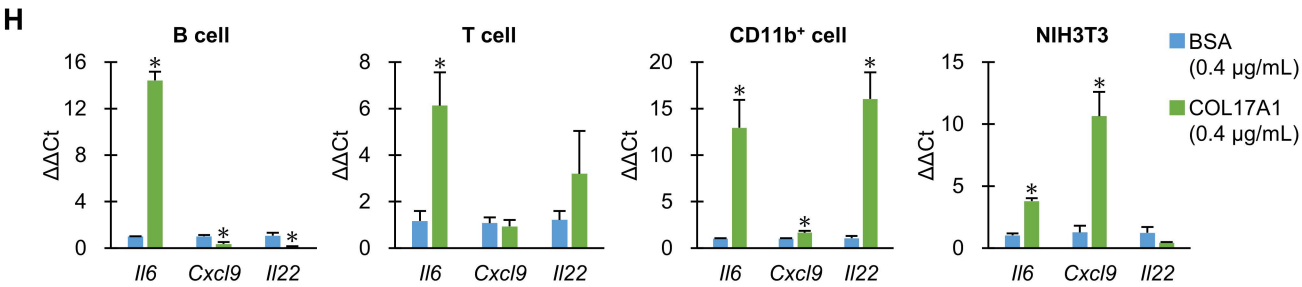

Supplemental Materials for

Close association between altered urine–urothelium barrier and tertiary lymphoid structure formation in the renal pelvis during nephritis

Osamu Ichii[1,2]*, Marina Hosotani[3], Md. Abdul Masum[1,4], Taro Horino[5], Teppei Nakamura[1,6], Takashi Namba[1], Yuki Otani[1,2], Yaser Hosny Ali Elewa[1,7], and Yasuhiro Kon[1]

1. Laboratory of Anatomy, Department of Basic Veterinary Sciences, Faculty of Veterinary Medicine, Hokkaido University, Sapporo, Japan 060-0818

2. Laboratory of Agrobiomedical Science, Faculty of Agriculture, Hokkaido University, Sapporo, Japan 060-8589

3. Laboratory of Anatomy, School of Veterinary Medicine, Rakuno Gakuen University, Ebetsu, Japan 069-8501

4. Department of Anatomy, Histology and Physiology, Faculty of Animal Science and Veterinary Medicine, Sher-e-Bangla Agricultural University, Dhaka, Bangladesh 1207

5. Department of Endocrinology, Metabolism and Nephrology, Kochi Medical School, Kochi University, Nankoku, Japan 780-8072

6. Section of Biological Safety Research, Chitose Laboratory, Japan Food Research Laboratories, Chitose, Japan 066-0052

7. Department of Histology, Faculty of Veterinary Medicine, Zagazig University, Zagazig, Egypt 44519

*Osamu Ichii (DVM, PhD)
Laboratory of Anatomy, Department of Basic Veterinary Sciences, Faculty of Veterinary Medicine, Hokkaido University, Kita 18, Nishi 9, Kita-ku, Sapporo 060-0818, Japan
Tel/Fax: +81-11-706-5189
Email: ichi-o@vetmed.hokudai.ac.jp

This PDF file includes:

Supplemental Tables 1 to 4
Supplemental Figures 1 to 15

Other supplemental materials for this manuscript include the following:

Supplemental Data 1 to 2 (provided by spreadsheet)

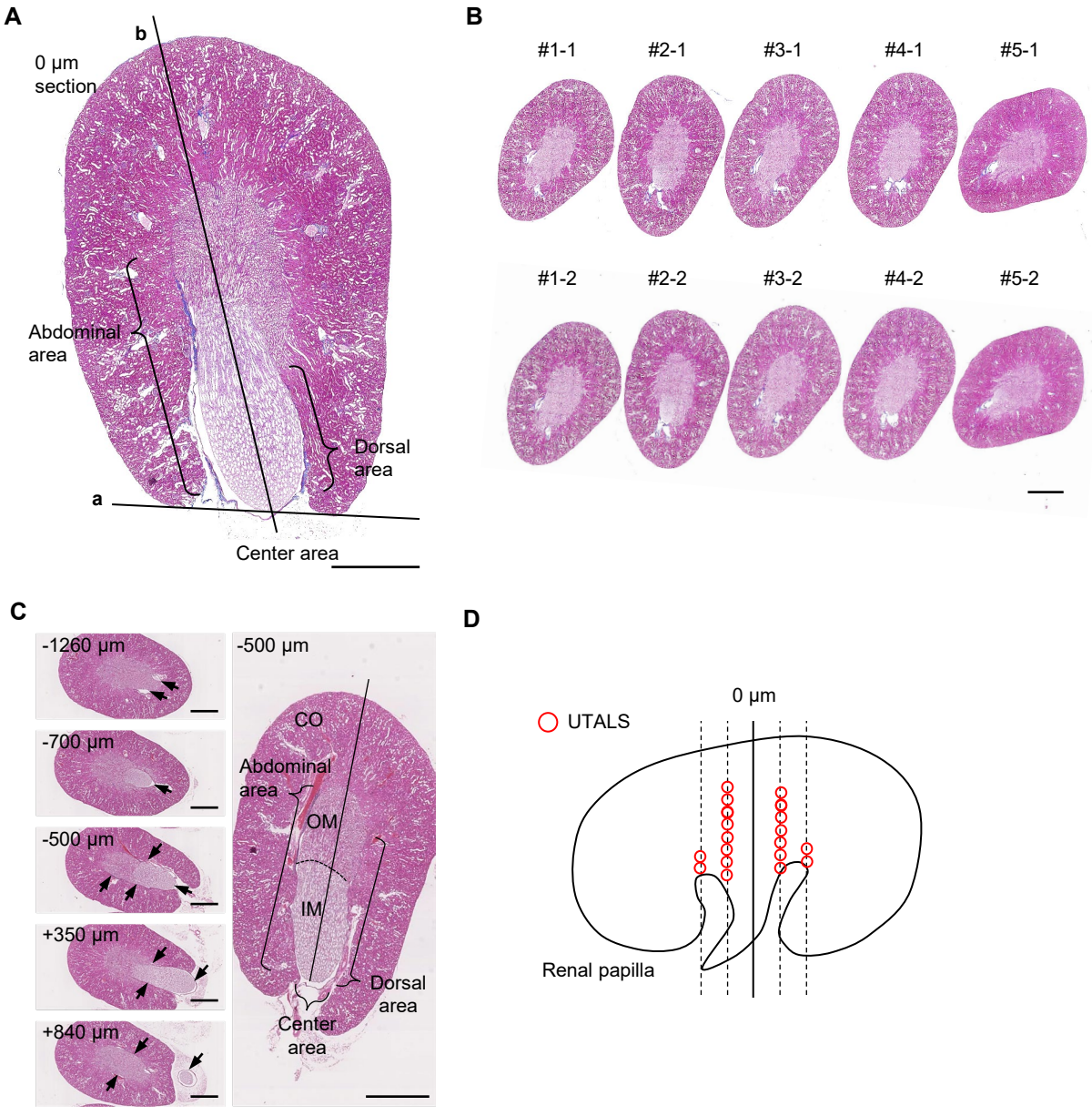

Supplemental Figure 1. Method used to localize the mouse lymphoid structures (LSs) formed in the renal pelvis (RP).

Six-month-old C57BL/6N were used in these experiments.

(A) Representative reference 0 μm section in semi-serial sections at 70 μm intervals. Sections showing similar levels of renal parenchyma and papilla (shown as line **a**) are defined as 0 μm sections. The lymphoid clusters found in line **b** are defined as LSs in the central area of the RP, while the others are defined as those in the abdominal or dorsal area of the RP; Masson's trichrome (MT) staining. These LSs are defined as urinary tract-associated lymphoid structures (UTALSs).

(B) Semi-serial sections. #1–5 indicate the individual number; MT staining.

(C) Summary of UTALS localization in the kidney. Arrows indicate the RP in semi-serial kidney sections. The number in the left corner indicates the distance from the reference section (0 μm); hematoxylin and eosin (H&E) staining.

(D) UTALS localizations considering RP morphology. Dotted straight lines indicate distance from the reference section (0 μm) at approximately 500 μm intervals. Red circles; UTALS.

Scale bars = 1 mm. CO, cortex; IM, inner medulla; OM, outer medulla.

A

	Abdominal						Center						Dorsal						Total number
μm	#1	#2	#3	#4	#5	SUM	#1	#2	#3	#4	#5	SUM	#1	#2	#3	#4	#5	SUM	
-1680	1			1	1	3					1	1				1	1	2	6
-1610	1	1		1	1	4				1		1				1	1	2	7
-1540	1	1				2					1	1	1		1	1		3	6
-1470	1	1	1			3					1	1	1	1	1			3	7
-1400	1	1	1		1	4				1		1	1	1	1			3	8
-1330	1	1	1			3				1	1	2	1	1	1			3	8
-1260	1	1	1			3				1	1	2	1	1	1			3	8
-1190	1	1	1			3				1	1	2	1	1	1			3	8
-1120		1	1			2	1	1		1	1	4		1	1			2	8
-1050			1			1	1	1		1	1	4			1			1	6
-980			1	1		2	1	1		1	1	4			1			1	7
-910			1	1		2	1	1		1	1	4			1		1	2	8
-840				1		1		1	1	1	1	4	1				1	2	7
-770				1		1	1	1	1	1	1	5	1				1	2	8
-700				1		1	1	1	1			3	1			1		2	6
-630				1		1	1	1	1		1	4			1	1		2	7
-560				1	1	2	1	1	1		1	4	1		1	1		3	9
-490	1			1	1	3	1	1	1		1	4	1	1	1	1		4	11
-420	1	1			1	3			1			1			1	1		2	6
-350		1			1	2				1		1			1			1	4
-280		1			1	2						0						0	2
-210		1				1				1		1						0	2
-140	1	1				2			1			1						0	3
-70		1		1		2						0						0	2
0			1	1		**2**						**0**						**0**	**2**
70				1		1						0						0	1
140						0						0						0	0
210						0						0					1	1	1
280	1		1			2						0						0	2
350				1		1	1					1	1					1	3
420						0	1			1		2						0	2
490	1	1		1		3	1			1	1	3	1	1		1		3	9
560	1	1		1		3	1			1	1	3	1	1		1	1	4	10
630			1	1		2	1	1	1	1	1	5			1	1	1	3	10
700					1	1		1	1	1	1	4	1				1	2	7
770		1				1		1	1	1	1	4	1	1				2	7
840		1			1	2		1	1	1		3		1				1	6
910		1			1	2		1	1	1		3		1				1	6

B

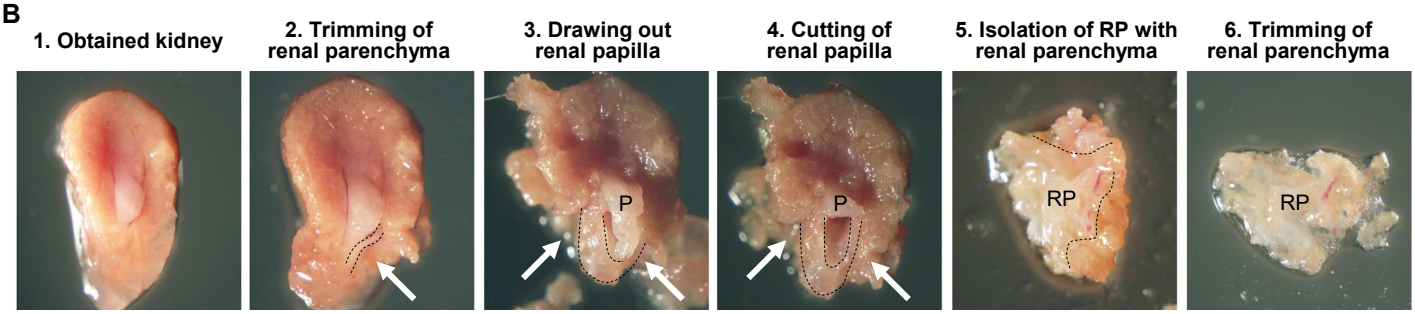

Supplemental Figure 2. Appearance of the mouse LSs formed in the RP and isolation of RP.
Six-month old C57BL/6N (n = 5) were used in these experiments.
(A) Summary of LS number found in the RP. These LSs are defined as urinary tract-associated lymphoid structures (UTALSs). Green indicates the presence of UTALSs, and red bars visualize the summation (SUM) of UTALS numbers in examined mice. Total number includes the number of UTALSs in abdominal, center, and dorsal areas of the RP of all examined mice.
(B) Isolation process of RPs from the kidney stored in RNAlater. Dotted lines indicate the border of RP. Arrows indicated the trimming area. P, renal papilla.

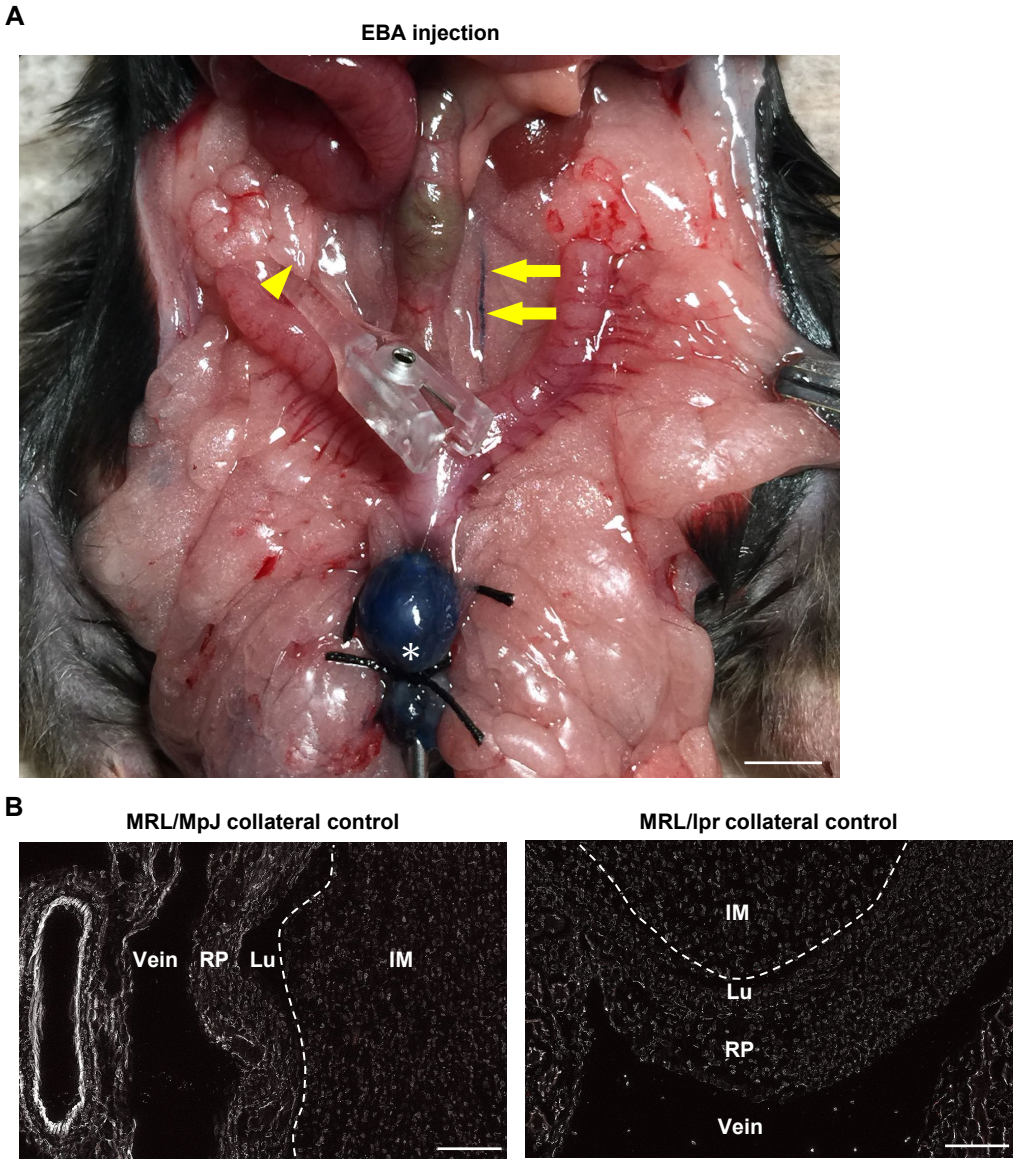

Supplemental Figure 3. *In vivo* methods for analyzing mouse urinary tract-associated lymphoid structures (UTALSs).

(A) Evans-blue-conjugated bovine serum albumin (EBA) injected into mouse renal pelvis (RP). The urethra was ligated and EBA was injected, in a retrograde manner, from the urinary bladder (asterisk) to the RP via the ureter (yellow arrows). The collateral ureter was clipped with a vascular clamp (yellow arrowhead). Six-month old C57BL/6N was used in this panel.

(B) Frozen sections of collateral control kidneys in EBA-injected mice. There is no red fluorescence derived from EBA. Dotted lines indicate the border between the inner medulla (IM) and lumen (Lu) of RP. The images of the injected side are shown in Figure 4G.

Scale bars = 1 cm (A), 50 μm (B).

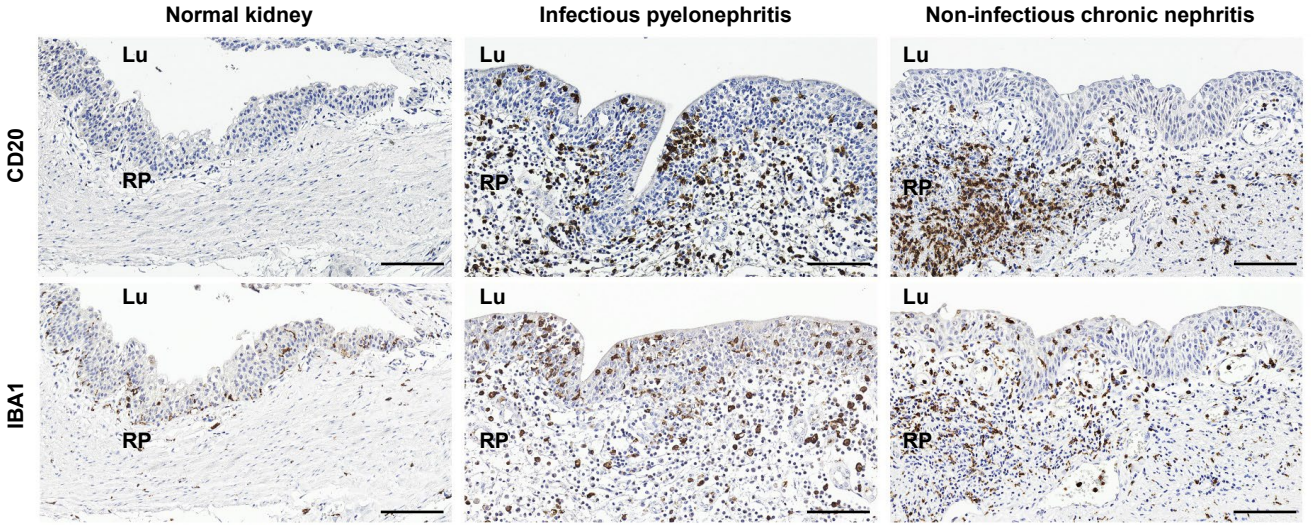

Supplemental Figure 4. Cell infiltration of the human renal pelvis with or without urinary tract infection.
Immunohistochemistry of $CD20^+$ B cells and $IBA1^+$ macrophages using necropsy samples of human kidneys showing normal histopathology (female, 33 years), infectious pyelonephritis (male, 39 years), and non-infectious chronic nephritis (male, 39 years). RP, renal pelvis; Lu, lumen of RP.
Scale bars = 100 μm.

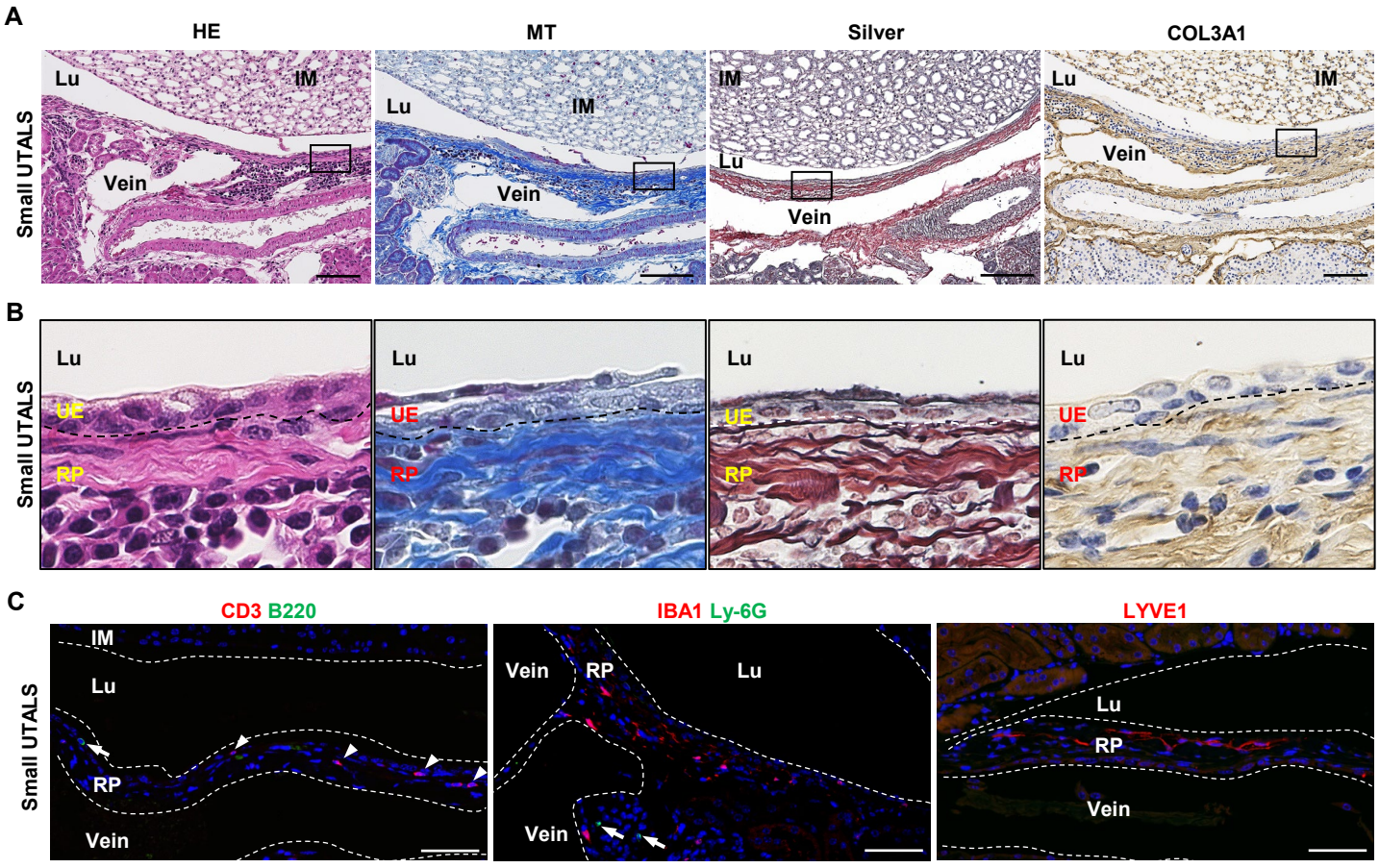

Supplemental Figure 5. Histology and cells composing small UTALSs in mice.
Six-month-old C57BL/6N were used.
(A) Representative features of small UTALSs visualized after H&E and MT staining, silver impregnation, and immunohistochemical staining for collagen type III alpha 1 (COL3A1).
(B) Magnified images of square area in (A). Dotted lines indicate the border between UE and parenchyma in the RP. Immune cells localize among well-developed collagen or reticular fibers. Doted lines indicate the border between the UE and RP parenchyma.
(C) Localization of $CD3^+$ T cells, $B220^+$ B cells, $Ly\text{-}6G^+$ granulocytes, $IBA1^+$ macrophages, and $LYVE1^+$ lymphatic vessels in small UTALSs. White dots indicate the border between the tissues and Lu or vein. Arrows indicate either $B220^+$ cells or $Ly\text{-}6G^+$ cells. Arrowheads indicate $CD3^+$ cells; immunofluorescence.
Scale bars = 100 μm (A), 50 μm (C). IM, inner medulla; Lu, lumen of RP; RP, renal pelvis; UE, urothelium.

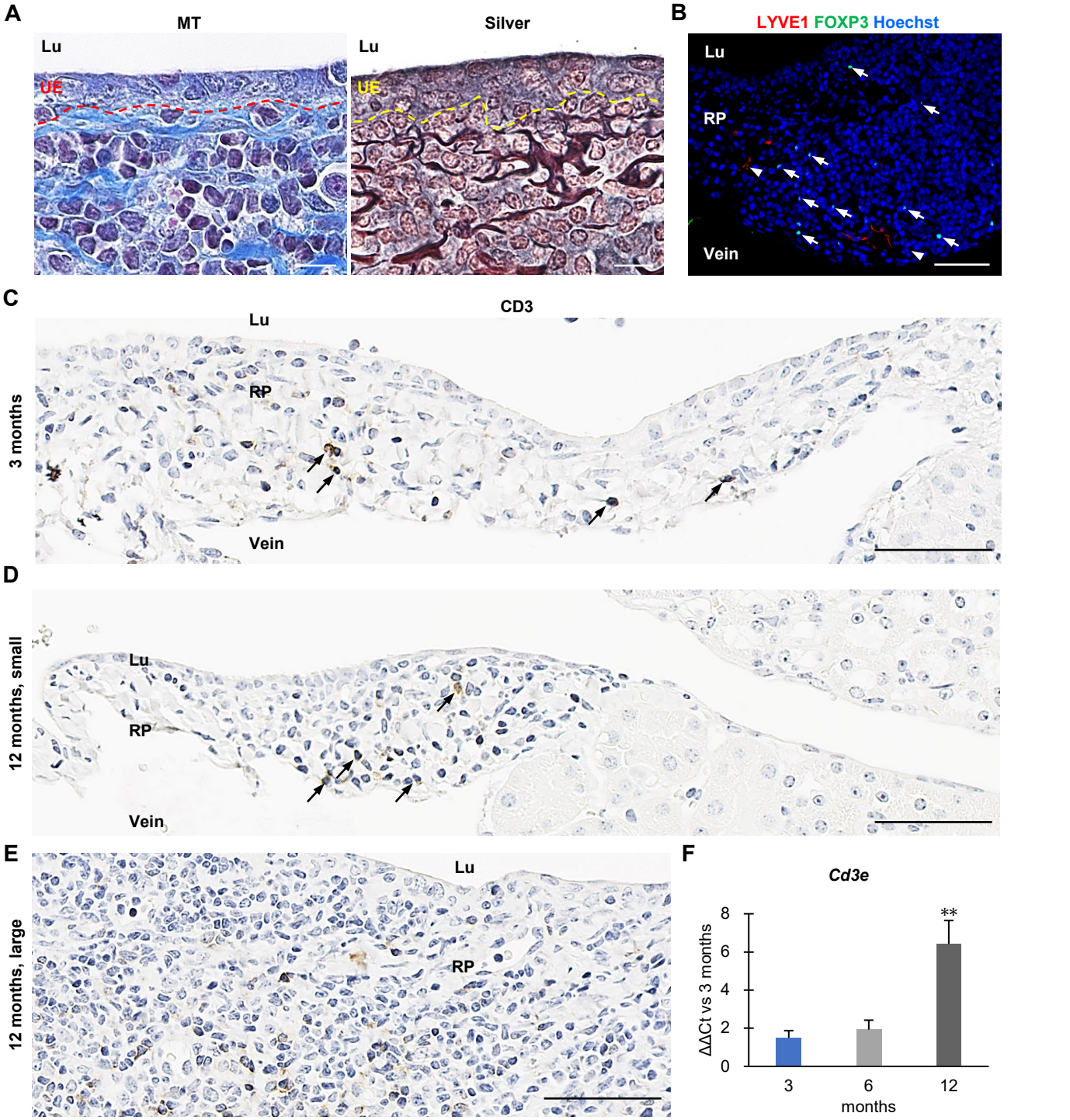

Supplemental Figure 6. Cell composition and age-related changes in the UTALSs of C57BL/6N.
Six-month-old (A, B), 3-month-old (C, F), 6-month-old (F), and 12-month-old (D-F) mice were used.
(A) Representative histological features of the fibers composing UTALSs visualized using MT staining and silver impregnation. Doted lines indicate the border between the UE and RP parenchyma.
(B) Localization of LYVE1$^+$ lymphatic vessels and FOXP3$^+$ regulatory T cells in UTALSs; immunofluorescence. Arrowheads indicate LYVE1$^+$ cells. Arrows indicate FOXP3$^+$ cells.
(C) Representative features of RPs at 3 months. Several mononuclear cells are observed and a few of them show CD3 positivity. Arrows indicate CD3$^+$ cells; immunohistochemistry.
(D, E) Representative features of RPs at 12 months. The development of UTALSs differs among individuals, and some of them showed small UTALSs (D) but others showed well-developed UTALSs (E); immunohistochemistry.
(**F**) *Cd3e* mRNA expression in RP.
Values are expressed as the mean ± SE. n = 6 (3 months) or 4 (6, 12 months) Significant differences compared with 3 months are indicated by $^{**}P$ <0.01; Dunnett's test. Scale bars = 50 μm (E). Scale bars = 10 μm (A), 50 μm (B-E). Lu, lumen of RP; RP, renal pelvis; UE, urothelium.

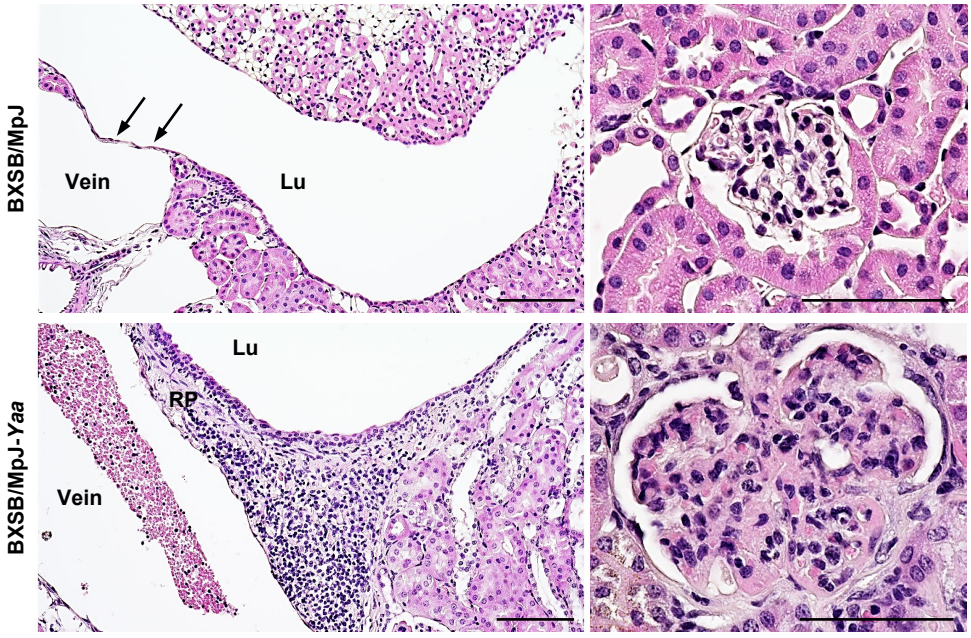

Supplemental Figure 7. Histology of UTALSs in spontaneous chronic glomerulonephritis mice.
UTALSs in a severe nephritis model mouse. Compared with BXSB/MpJ healthy control at 6 months, same aged BXSB/MpJ-*Yaa* show well-developed UTALSs in the RP with severe glomerulonephritis (right panels). The RP of BXSB/MpJ is thin (arrows); H&E staining.
Scale bars = 100 μm (left panels), 50 μm (right panels). Lu, lumen of RP; RP, renal pelvis.

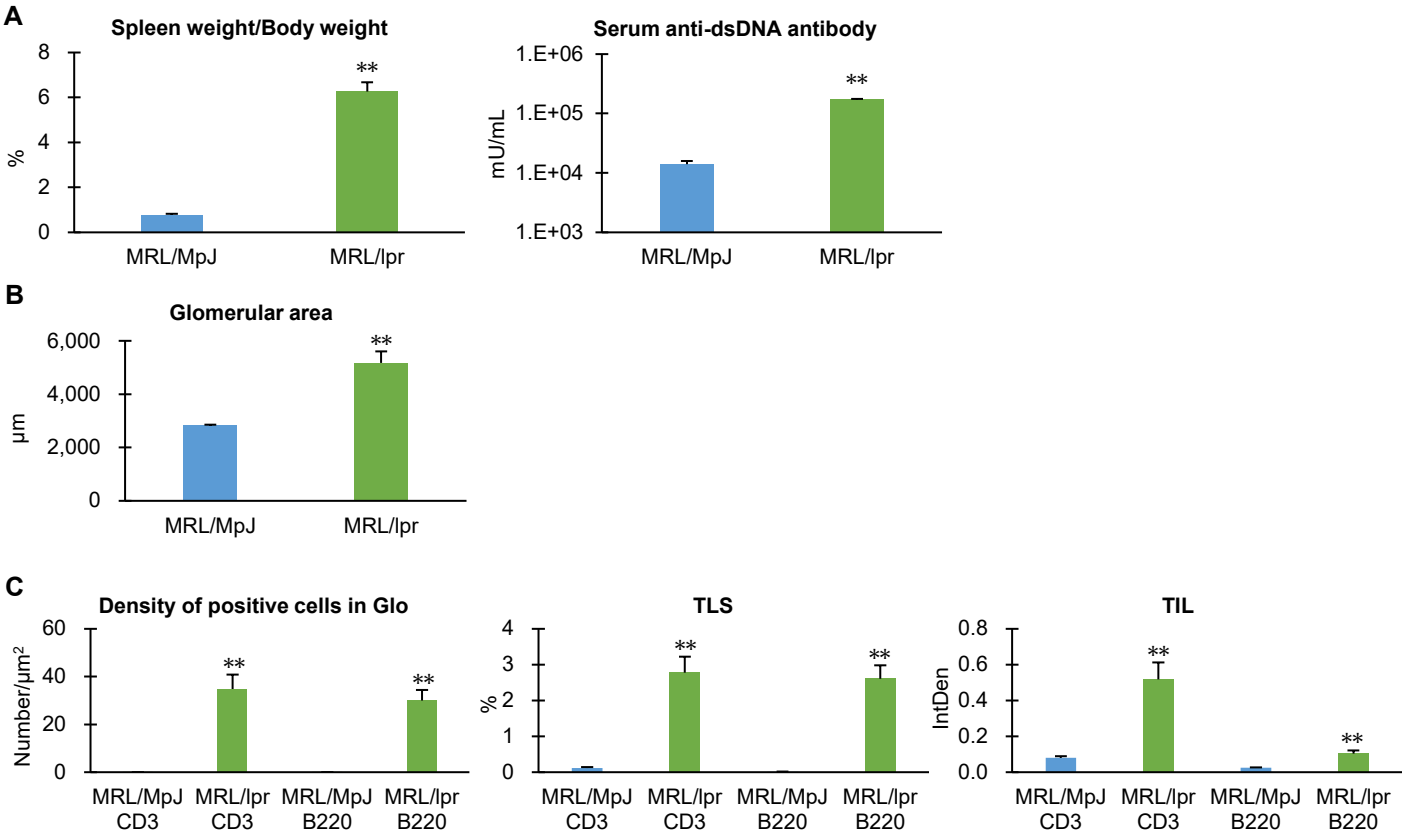

Supplemental Figure 8. Indices for abnormalities of systemic immune conditions and renal histopathology in healthy and a non-infectious nephritis mouse model.

Six-month-old MRL/MpJ and MRL/lpr were used for these experiments.

(A–C) Pathological indices for systemic immune conditions (A), glomerular area (B), and renal histopathology targeting $CD3^+$ T cells and $B220^+$ B cells (C).

Values are shown as mean ± SE; n = 7 or 10 (MRL/MpJ or MRL/lpr). Significant differences between strains are indicated by $^{**}P$ <0.01; Mann–Whitney U-test. dsDNA, double stranded DNA; Glo, glomerulus; TIL, tubulointerstitial lesion; TLS, tertiary lymphoid structure.

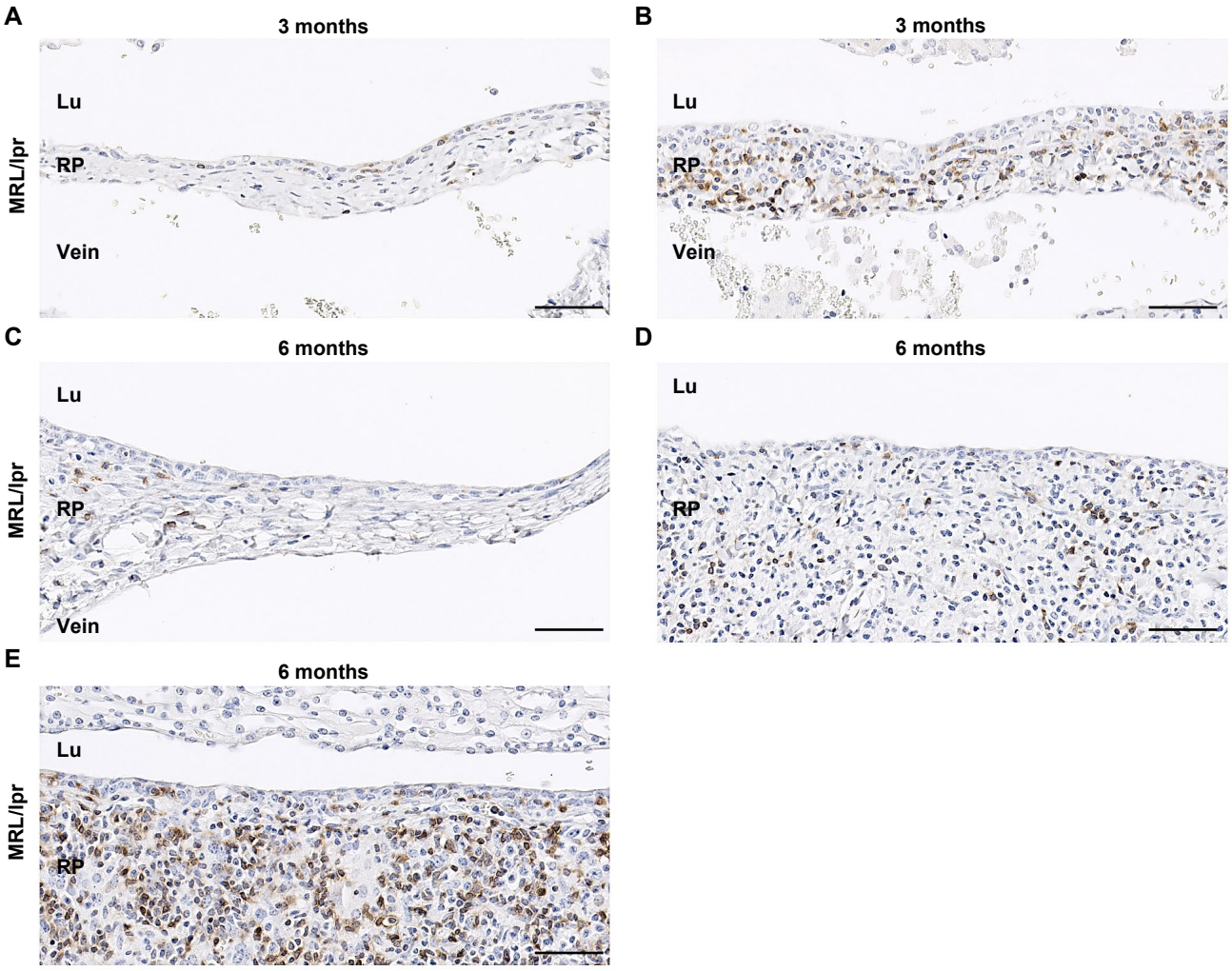

Supplemental Figure 9. Age-related changes in the UTALSs of MRL/lpr.
Immunohistochemical staining for CD3.
(A, B) Representative features of renal pelvises (RPs) at 3 months. Several mononuclear cells can be observed and a few of them show CD3 positivity (A). In several mice, moderately developed UTALSs were found in RPs (B).
(C-E) Representative features of RPs at 6 months. The development of UTALSs differed among individuals and some of them showed small or larger UTALSs (A and B). Several mice showed well-developed UTALSs in RPs (E).
Scale bars = 50 μm. Lu, lumen of RP.

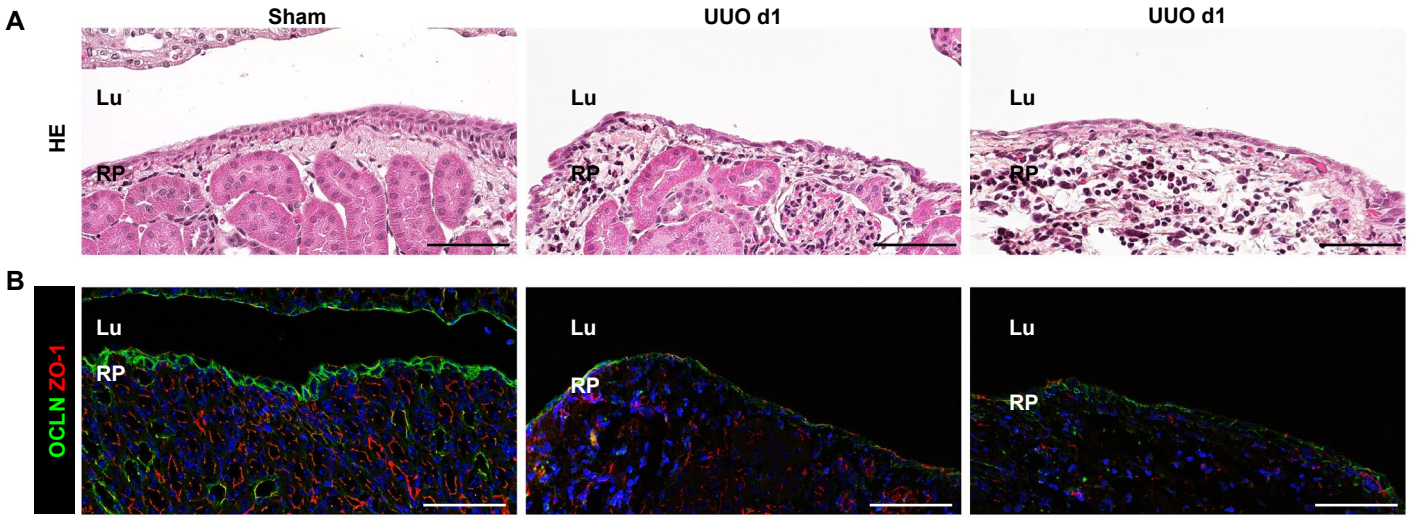

Supplemental Figure 10. Histopathological changes in mouse renal pelvis (RP) after unilateral ureter obstruction (UUO).

(A) Eight-week-old C57BL/6N was used and their RPs were analyzed after 1 day (d1) of sham operation or UUO. Histological features of RP. In sham-operated mice, the urothelium of RP was intact and the number of infiltrating cells was negligible. After UUO, thinning of the urothelium was partially observed, and the severity of cell infiltration differed among individuals or RP portions; H&E staining.

(B) Localization of OCLN and ZO-1 in the urothelium of the RP. The RPs of sham-operated mice showed clear, positive reactions of OCLN and ZO-1 in the urothelium. These reactions were weak in UUO mice; immunofluorescence.

Scale bars = 50 μm. Lu, lumen of RP.

A

Pathway GO. ID	Pathway description	Gene count	FDR
0002682	Regulation of immune system process*	110	1.3E-18
0002376	Immune system process*	135	5.8E-18
0065007	Biological regulation	469	7.0E-16
0007155	Cell adhesion	92	3.4E-14
0051239	Regulation of multicellular organismal process	172	4.9E-14
0030154	Cell differentiation	213	1.0E-13
0002684	Positive regulation of immune system process*	71	1.8E-13
0007154	Cell communication	237	2.2E-13
0044707	Single-multicellular organism process	300	2.2E-13
0050789	Regulation of biological process	441	3.3E-13

B

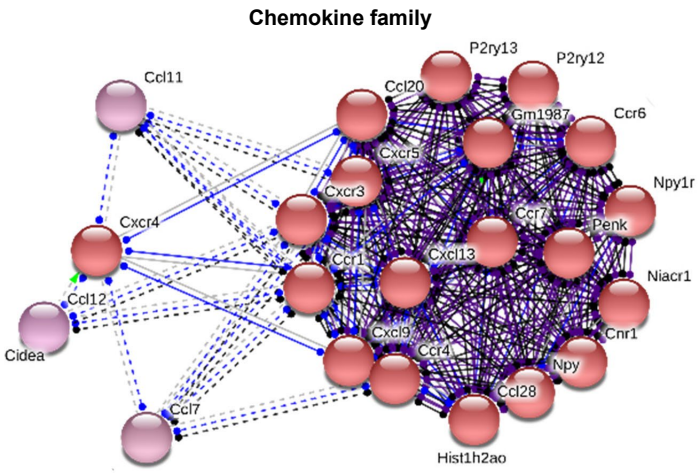

C

		MRL/MpJ RP vs MRL/MpJ kidney		MRL/lpr RP vs MRL/MpJ RP	
	Rank	Symbol	Ratio	Symbol	Ratio
Ccl	1	*Ccl20*	22.9	*Ccl1*	10.2
	2	*Ccl8*	16.3	*Ccl20*	7.2
	3	*Ccl1*	9.8	*Ccl21a*	5.0
	4	*Ccl12*	8.9	*Ccl8*	4.3
	5	*Ccl11*	4.3	*Ccl19*	4.1
Cxcl	1	*Cxcl13*	6.9	*Cxcl9*	4.2
	2	*Cxcl9*	6.4	*Cxcl13*	2.6
	3	*Cxcl14*	2.2	*Cxcl10*	1.7
	4	*Cxcl10*	2.1	*Cxcl12*	1.5
	5	*Cxcl17*	1.9	*Cxcl14*	1.4
Ccr	1	*Ccr6*	10.6	*Ccr6*	5.8
	2	*Ccr7*	4.0	*Ccr10*	4.3
	3	*Ccr1*	3.5	*Ccr4*	4.2
	4	*Ccr4*	3.5	*Ccr7*	3.5
	5	*Ccr7*	2.7	*Ccr9*	3.1
Cxcr	1	*Cxcr5*	16.1	*Cxcr5*	3.9
	2	*Cxcr3*	4.4	*Cxcr4*	3.6
	3	*Cxcr4*	3.0	*Cxcr3*	3.4
	4	*Cxcr6*	2.5	*Cxcr6*	2.4
	5	*Cxcr2*	0.9	*Cxcr1*	0.7

Supplemental Figure 11. Chemokine family expression in mouse RP.
Six-month-old MRL/MpJ and MRL/lpr were used as healthy controls and a non-infectious chronic nephritis mouse model, respectively.
(A) Molecular pathway-targeting biological processes associated with mouse UTALS development. Based on the obtained microarray data (Supplemental data 1), 1,108 genes showing 3-fold higher expression in the RPs than in the kidneys of in MRL/MpJ mice were analyzed. The top ten significant pathways for each enrichment are listed. FDR, false discovery rate. Asterisks: immune-associated gene ontology terms.
(B) Molecular cluster targeting chemokine family. Based on microarray data (Supplemental data 1), 1,108 genes showing 3-fold higher expression in RPs compared with that in the kidney of MRL/MpJ mice at 6 months of age were analyzed using STRINGs (https://string-db.org/).
(C) Relative gene expression of chemokine ligands or their receptors in the RP compared with in the kidneys; microarray analysis. The top five highly expressed genes for chemokine ligands and their receptors are listed.

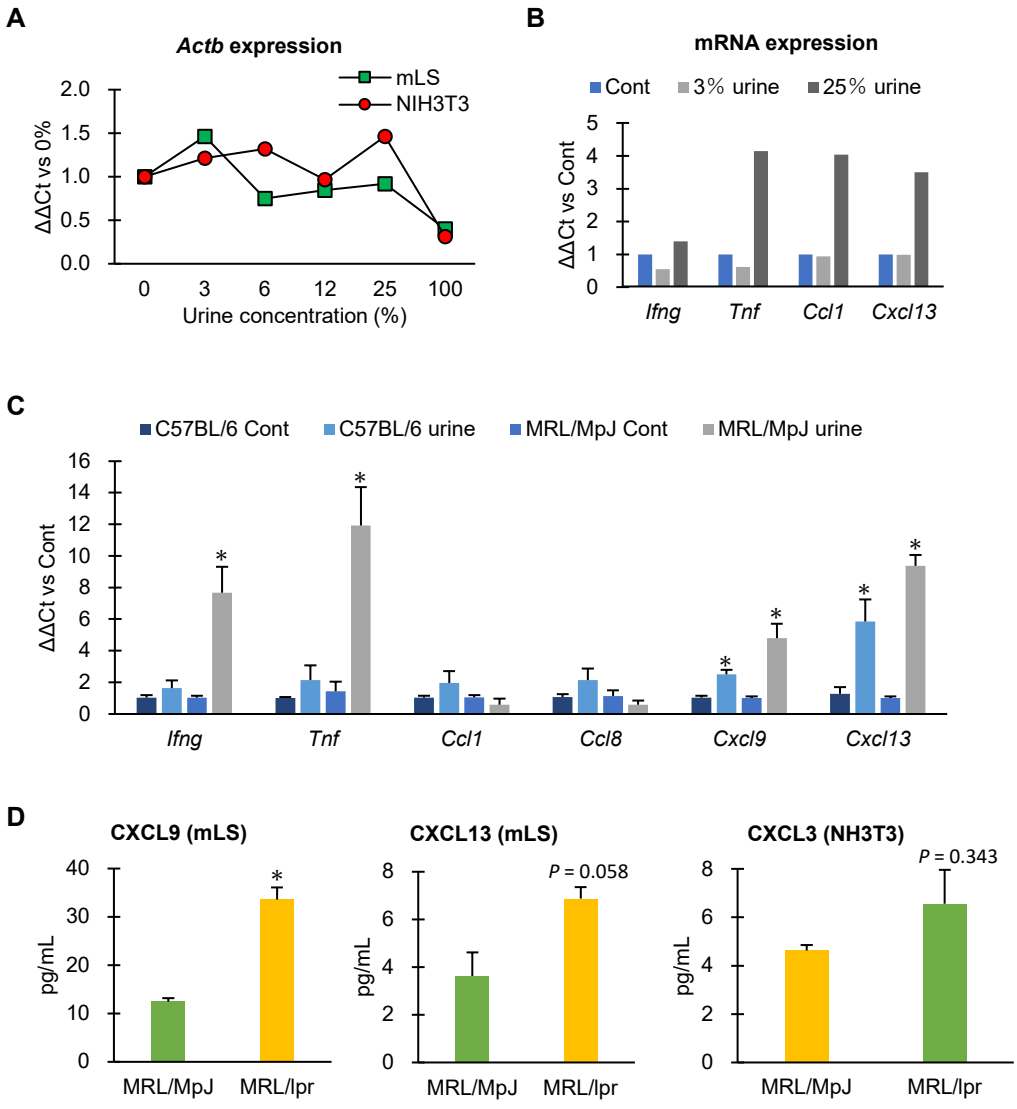

Supplemental Figure 12. Housekeeping gene and chemokine gene expression in cultured cells after stimulation by mouse urine.

(A) Gene expression of actin beta (*Actb*) used as a housekeeping gene in mimic lymphoid structures (mLSs) of C57BL/6N mice and NIH3T3 cells.

(B, C) Cytokine/chemokine gene expression in mLSs of C57BL/6N (B) and C57BL/6N or MRL/MpJ (C) after stimulation with their urine.

(D) Culture supernatant levels chemokines in MRL/MpJ-derived mLSs after stimulation with 25% MRL/MpJ or MRL/lpr urine for 4 h.

n = 1 (A, B), 4 (C, D). Significant differences between PBS control (Cont) and urine (A-C) or MRL/MpJ and MRL/lpr (D) mice are indicated by **P* <0.05, Mann–Whitney *U*-test (C, D); qPCR analysis (A-C), ELISA (D).

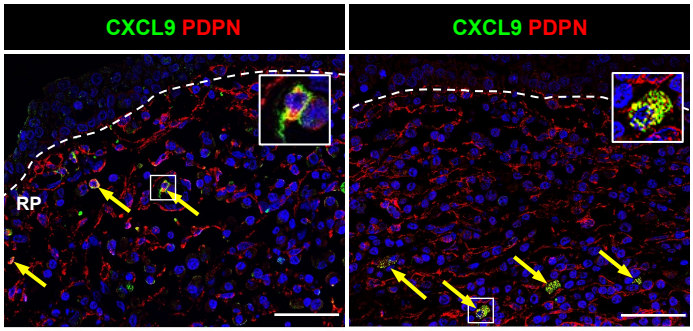

Supplemental Figure 13. CXCL9 or CXCL13-expressing fibroblasts in the human RP showing infectious pyelonephritis.

Arrows indicate the localization of CXCL9$^+$ or CXCL13$^+$ and PDPN$^+$ fibroblasts in the RP of a human kidney with infectious pyelonephritis (male, 39 years). White dots indicate the border between the urothelium and RP parenchyma; immunofluorescence.

Scale bars = 50 µm.

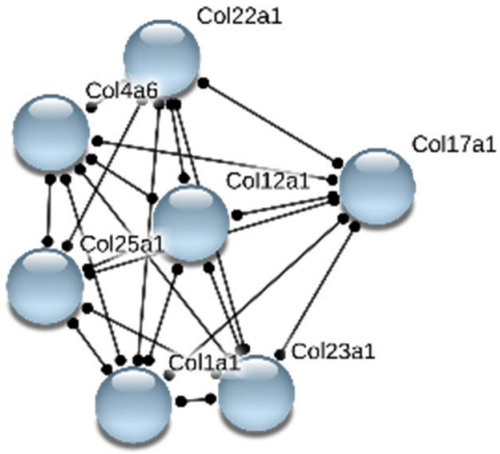

Supplemental Figure 14. Collagen family expression in the mouse RP.
Molecular clusters targeting collagen family. Based on microarray data (Supplemental data 1), 1,108 genes showing 3-fold higher expression in RPs than in the kidneys of MRL/MpJ at 6 months of age were analyzed using STRINGs (https://string-db.org/).

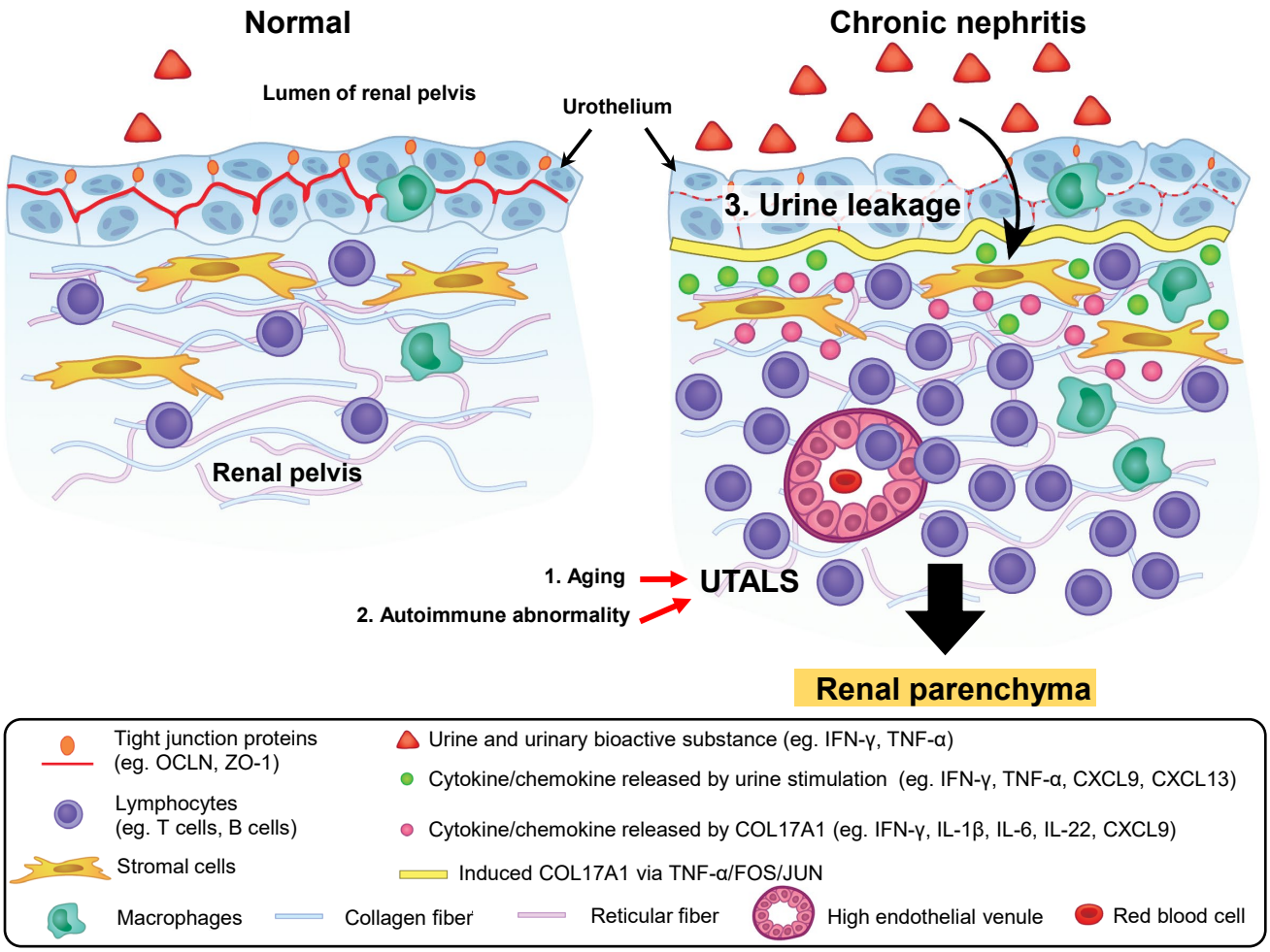

Supplemental Figure 15. Formation of UTALSs in the RP is associated with alterations in the urine–urothelium barrier.

Urine leakage from the RP lumen into its parenchyma via the urothelial barrier—which is altered by bioactive factors from the urine and RP parenchyma—stimulates RP stromal cells immunologically and attracts immune cells by producing cytokine/chemokines. COL17A1 production induced in the urothelium by the activated FOS/JUN pathway is also involved in these processes. UTALSs are strongly associated with the progression of chronic nephritis, regardless of urinary tract infection.